Large earthquake cycles and intermittent criticality on heterogeneous faults due to evolving stress and seismicity

Yehuda Ben-Zion
Department of Earth Sciences, University of Southern California, Los Angeles, California, USA

Mariana Eneva
Science Applications International Corporation, San Diego, California, USA

Yunfeng Liu
Department of Earth Sciences, University of Southern California, Los Angeles, California, USA

Received 30 July 2002; revised 27 January 2003; accepted 28 February 2003; published 19 June 2003.

[1] We analyze evolving stress and seismicity generated by three realizations of a discrete model of a strike-slip fault in a three-dimensional (3-D) elastic half space using five functions of stress and five functions of seismicity. The first model (F) has realistic dynamic weakening (static minus dynamic frictions), the second (FC) has zero critical dynamic weakening, and the third (SYS) is constrained to produce only system size events. The results for model F show cyclical development, saturation, and destruction of fluctuations and long-range correlations on the fault, punctuated by the system size events. The development stage involves evolution of stress and seismicity to distributions having broad ranges of scales, evolution of response functions toward scale-invariant behavior, increasing seismicity rate and event sizes, and increasing hypocenter diffusion. Most functions reach asymptotically stable values around 2/3 of the cycle and then fluctuate until one event cascades to become the next large earthquake. In model FC the above evolution is replaced by scale-invariant statistical fluctuations, while in model SYS the signals show simple cyclic behavior. The results suggest that large earthquake cycles on heterogeneous faults with realistic positive dynamic weakening are associated with intermittent criticality, produced by spontaneous evolution of stress heterogeneities toward a critical level of disorder having a broad range of scales. The stress evolution and development of large earthquake cycles may be tracked with seismicity functions. *INDEX TERMS:* 3220 Mathematical Geophysics: Nonlinear dynamics; 7209 Seismology: Earthquake dynamics and mechanics; 7223 Seismology: Seismic hazard assessment and prediction; 7260 Seismology: Theory and modeling; 8164 Tectonophysics: Stresses—crust and lithosphere; *KEYWORDS:* Earthquake physics, heterogeneous faults, evolving stress, seismicity patterns, intermittent criticality, prediction

Citation: Ben-Zion, Y., M. Eneva, and Y. Liu, Large earthquake cycles and intermittent criticality on heterogeneous faults due to evolving stress and seismicity, *J. Geophys. Res.*, *108*(B6), 2307, doi:10.1029/2002JB002121, 2003.

1. Introduction

[2] Earthquake prediction would be a simple matter if rheological properties and stress evolution on a fault were precisely known. In the last few decades there has been considerable progress in developing a detailed frictional framework for the inception of brittle failures in the seismogenic crust [e.g., *Byerlee*, 1978; *Dieterich*, 1992; *Scholz*, 2002]. However, the other pair member required for completing the mechanical description, the stress, is, in general, not an observable quantity. It is important to search with model calculations for appropriate surrogate variables that can track the stress evolution on a fault. Such variables may be useful for developing an improved strategy for forecasting large events. In the present work we attempt to quantify the spatiotemporal evolution of stress on a heterogeneous fault in relation to seismicity using the discrete model of *Ben-Zion* [1996] for a two-dimensional (2-D) segmented strike-slip fault in a 3-D elastic half space (Figure 1a). The model is sufficiently realistic to produce stress and seismicity patterns that are likely to be relevant to natural faulting, yet simple enough to allow some analytical understanding and efficient numerical calculations.

[3] *Ben-Zion* [1996] suggested on the basis of qualitative comparisons of stress distributions at different times that during gradual tectonic loading, small and intermediate size earthquakes produce stress roughening over their size scales, which collectively smooth the longer wavelength components of stress and prepare the fault for the occur-

0148-0227/03/2002JB002121$09.00

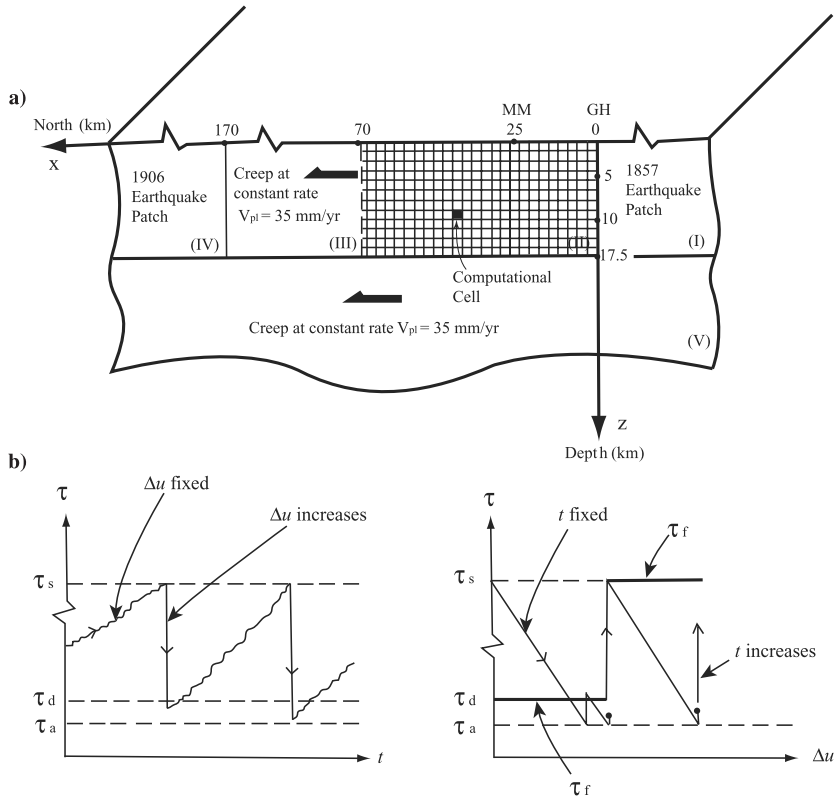

Figure 1. (a) A planar representation of a 3-D segmented fault zone by a 2-D heterogeneous fault embedded in a 3-D elastic half-space. The geometric disorder is modeled as disorder in strength properties of the planar fault. On regions I, III, IV, and V, boundary conditions are specified. Region II is a computational grid where spatiotemporal evolution of stress and slip are calculated. The shown model configuration is tailored for the central San Andreas Fault. GH and MM mark approximate positions of Gold Hill and Middle Mountain. (b) Schematic diagrams of stress versus time and stress versus slip at the center of computational cells. Static strength, dynamic strength, arrest stress, and failure threshold are denoted by τ_s, τ_d, τ_a, and τ_f, respectively [from *Ben-Zion and Rice*, 1993; *Ben-Zion*, 1996].

rence of a large event. The pattern is reversed during large ruptures of size approaching the system dimension, which reduce the stress level and smooth the fluctuations along the large rupture area, while creating large stress concentrations near its boundary and increasing the stress outside it [*Ben-Zion*, 1996, Figures 8–11]. In the language of critical phenomena, the smoothing of long wavelength stress fluctuations in the evolutionary stage preceding large earthquakes corresponds to the development of long-range stress correlations [e.g., *Sornette and Sammis*, 1995]. The system-sized events that reroughen the long wavelength stress field on the fault destroy the long-range correlations and set the beginning of a new large earthquake cycle. In the following sections this process is analyzed quantitatively with various stress and seismicity variables. To provide a context for the analysis, we first summarize briefly key model attributes and previous results relevant to our work.

[4] The model contains a computational grid (region II of Figure 1a) where evolving stress and seismicity are generated in response to ongoing loading imposed as slip boundary conditions on the other fault regions. Boundary conditions play a fundamental role on the resulting dynamics and it is important to use conditions that mimic those operating on natural faults. Following *Ben-Zion and Rice* [1993], the model boundary conditions and geometry are chosen to represent deformation along the central San Andreas fault. Regions III and V creep at constant plate velocity of 35 mm/yr, while regions I and IV follow staircase slip histories with recurrence times of 150 yr. The stress transfer due to the imposed boundary conditions and failing grid cells is calculated using a discretized form of a boundary integral equation employing the static solution of *Chinnery* [1963] for dislocations in a 3-D elastic half space. The employed boundary conditions produce, together with the elastic stress transfer function, space- (and time-) dependent loading, with strong stress concentrations or "shielding" near the edges of the computational grid. Strong stress concentration at the bottom of the brittle seismogenic zone is a general realistic feature of crustal faults. Stress concentrations and shielding along strike due to failing and locked portions of faults are also general realistic features, although not necessarily in the particular form used here.

[5] Deformation at each computational cell is the sum of slip contributions from brittle and creep processes. The brittle process (Figure 1b) is governed by distributions of static friction τ_s, dynamic friction τ_d, and arrest stress τ_a. The static friction characterizes the brittle strength of a cell until its initial failure in a given model earthquake. When stress τ at a cell reaches the static friction, the strength drops to the dynamic friction for the remaining duration of the

event. The stress at a failing cell drops to the arrest level τ_a, which may be lower than τ_d to accommodate dynamic overshoot, producing local slip governed by the Chinnery's solution. The static friction, dynamic friction, and arrest stress are connected via a dynamic overshoot coefficient $D = (\tau_s - \tau_a)/(\tau_s - \tau_d)$. If the stress transfer from failing regions increases the stress at other cells to their static or dynamic strength thresholds, as appropriate, these cells fail and the event grows. When the stress at all cells is below the brittle failure thresholds, the model earthquake ends and the strength at all failing cells recovers back to τ_s. The creep process is governed by a power law dependency of creep velocity on the local stress and space-dependent coefficients that increase exponentially with depth and with distance from the southern edge of the computational grid. The chosen parameters produce an overall "pine tree" stress-depth profile with a "brittle-ductile" transition at a depth of about 12.5 km, and variable stress-along-strike profiles with a "brittle-creep" transition around 65 km NW of the 1857 rupture (see *Ben-Zion* [1996] and *Ben-Zion and Rice* [1993] for additional details).

[6] *Fisher et al.* [1997] and *Dahmen et al.* [1998] studied a simplified version of the model with a constant mean field stress transfer instead of the $1/r^3$ elastic dependency on distance r from the source, without the creep process in the computational grid, and with creeping boundary conditions everywhere else (regions I, III, IV, and V). Using renormalization group theory, analysis of Bernoulli process and computer simulations, they mapped analytically and numerically the dynamics of the model to a phase diagram spanned by two tuning parameters: a dynamic weakening coefficient $\varepsilon = (\tau_s - \tau_d)/\tau_s$ and a conservation parameter of stress transfer C. (Note that for finite stress drops $\tau - \tau_a$ and zero dynamic weakening $\varepsilon = 0$, the dynamic overshoot coefficient D is unbounded.) *Fisher et al.* [1997] found that the model has an underlying critical point of a phase transition at zero dynamic weakening and full conservation of stress transfer. Since the response of a system with tuning parameters at critical values is scale-invariant, model simulations with $\varepsilon = 0$, $C = 1$ should produce power law statistics and time histories with fractal-like fluctuations. This limit response is illustrated and used in sections 3 and 4, where we attempt to characterize the dynamical structure of simulation results for the general case of tuning parameters not fixed at critical values.

[7] *Dahmen et al.* [1998] showed that in addition to criticality, the model has different types of dynamic behavior for different ranges of values of ε and C, including a regime with truncated power law frequency-size statistics of earthquakes and a regime with mode-switching behavior. The latter consists of self-driven fluctuations between time intervals associated with relatively high seismic release and frequency size statistics compatible with the characteristic earthquake distribution, and time intervals with relatively low seismic release and truncated power law frequency size statistics. See also *Ben-Zion et al.* [1999] and *Zöller et al.* [2003]. Since the model has different dynamic regimes for different parameter values, it is not compatible with "self-organized criticality" where there are no tuning parameters [e.g., *Main*, 1996; *Jensen*, 1998].

[8] Extensive numerical simulations with several different classes of models, summarized by *Ben-Zion* [2001], suggest that the degree of disorder in fault heterogeneities is another tuning parameter of the dynamics. Simulations with smooth homogeneous systems produce typically a limited range of event sizes [e.g., *Rice*, 1993; *Ben-Zion and Rice*, 1995, 1997; *Shaw and Rice*, 2000], while simulations with strong heterogeneities generate broad frequency size statistics of earthquakes with some power law range [e.g., *Ben-Zion and Rice*, 1993, 1995; *Lyakhovsky et al.*, 2001]. In general, the ability of initial failure events to propagate and grow depends on the existing distributions of strength and stress, or more precisely on the difference between the two (i.e., the stress deficit). In the present model, the strength properties are quenched but the stress distributions (and hence the difference between strength and stress) evolve with time. The lack of analytical understanding of the effects of heterogeneities does not allow us to fine tune the strength heterogeneities to produce very closely an expected behavior (e.g., criticality), as can be done with ε and C. Nevertheless, *Ben-Zion and Rice* [1993, 1995] and *Ben-Zion* [1996] showed that the range of size scales characterizing the distribution (not necessarily a power law) of brittle fault properties correlates with the power law range of frequency size event statistics.

[9] The results of the present work indicate that during a large earthquake cycle on a heterogeneous fault with tuning parameters not at critical values, the stress evolves to a distribution having a wide range of scales, thus bringing dynamically the fault closer to a critical level of disorder. This evolutionary stage is associated with increasing stress fluctuations, transfer of stress power spectra from long to small wavelengths, development of scale-invariant behavior of response functions, increasing seismicity rate and maximum earthquake size, increasing power law range of frequency size event statistics, increasing diffusion and decreasing average depth of hypocenter locations, and development of long-range correlations of stress and seismicity. During large system-sized events these trends are reversed, leading to an overall evolution that may be characterized as cyclical nonrepeating approach to and retreat from criticality or intermittent criticality. The accompanying seismicity evolution over increasing length scales forms a reversed cascade of events to that of turbulence.

[10] Details of the above pattern may be used to provide an improved understanding of various stages of large earthquake cycles on heterogeneous faults. Some of the examined stress and seismicity functions reach asymptotically stable values around 2/3 of the cycle and then fluctuate, while others continue to increase more slowly, until one small event cascades to become the next large earthquake. The evolutionary stage with increasing trends can be considered interseismic with low probably for the occurrence of a large earthquake, while the stage following the establishment of several extrema may be referred to as preseismic with increased large earthquake probability. Continuing analysis with synthetic and observed data may clarify further the dynamics of large earthquake cycles and lead to the development of improved strategy for forecasting large seismic events.

2. Analysis Techniques

2.1. Overview and Model Realizations

[11] To quantify the evolution of stress on a fault in relation to seismicity and criticality, we calculate the tem-

poral variations of five functions of stress and five functions of seismicity using 150 years long histories simulated by three model realizations. One model (F) has realistic properties and response functions, while the other two (FC and SYS) are "control" cases that allow us to examine changes in the dynamics associated with tuning parameters and ongoing seismicity. In all models, the employed computational cells are squares with a dimension of 0.55 km, the creep properties are as used by *Ben-Zion* [1996, Figure 3], and the calculations are done with full conservation of stress transfer ($C = 1$). To reduce effects associated with large stress concentrations at the edges of the computational grid, the stress analysis is done on the central part of the seismogenic zone in the fault region 7.5 km $< x <$ 62.5 km, 4 km $< z <$ 8 km. The seismicity functions are calculated over the entire computational grid. To focus on temporal variations, the initial stress distribution is subtracted from the stress values at subsequent times.

[12] The three model realizations have different brittle properties as follows:

[13] 1) Model F has uniform static coefficient of friction of 0.75, fractal distribution of arrest stress characterized by fractal dimension 2.3, mean value 0.5, and standard deviation 0.2, finite dynamic overshoot coefficient $D = 1.25$, and corresponding (spatially variable) positive dynamic weakening coefficient $\varepsilon > 0$. The static friction increases linearly with depth following an overburden gradient of 18 MPa/km, the average value of $\tau_s - \tau_a$ along the fault is 3.3 MPa, and the dynamic friction at each position is $\tau_d = \tau_s + (\tau_s - \tau_a)/D$ (see *Ben-Zion* [1996] for additional details). This model with heterogeneous distribution of brittle stress drops and noncritical dynamic weakening (finite ε and D values) represents a general case and is the primary target for the analysis.

[14] 2) Model FC has the same static friction and arrest stress distributions as model F, but a critical value of dynamic weakening coefficient $\varepsilon = 0$ (i.e., $\tau_d = \tau_s$). This case is used to distinguish evolution of dynamical structures characterizing results associated with large earthquake cycles in systems with tuning parameters not fixed at critical values, from scale-invariant structures expected to exist in cases with tuning parameters at critical values.

[15] 3) Model SYS has the same static friction as model F, uniform arrest stress $\tau_s - \tau_a = 20$ MPa, finite dynamic overshoot coefficient $D = 1.1$ (and related finite $\varepsilon > 0$), and a feature that produces only system-sized events. The latter is done by reducing the friction to the dynamic value everywhere on the computational grid after a brittle event starts at any position. This model is used to distinguish collective evolution associated with realistic ongoing population of seismicity on a fault from simpler evolution associated only with overall stress cycling due to continuous (space-dependent) loading and occasional large earthquakes.

[16] The stress functions can be calculated at individual times, over given time intervals, or for groups of events. The latter two options involve averaging and produce smoother results. The seismicity functions require populations of earthquakes, which exist only in cases F and FC, and are calculated for groups with a constant number (100) of events. To enable comparisons between results of model SYS with the other cases, the stress functions are first calculated in section 3 at individual times. In section 4 the stress and seismicity functions are calculated for event groups to allow comparisons between the evolution of the two sets of functions in models F and FC.

2.2. Stress Functions

[17] The five employed stress functions are:

[18] 1) Average stress on the fault

$$AS(t) = \frac{1}{N}\sum_{i=1}^{N}\tau_i(t), \tag{1a}$$

where $\tau_i(t)$ is the stress at cell i and time t minus initial stress at the same position. The average stress tracks evolution associated with the remote loading. In cases with tuning parameters not fixed at critical values, the average stress provides a simple illustration of large earthquake cycles. In systems with tuning parameters at critical values, the average stress and all other functions are scale-invariant and hence do not have cyclical components related to large earthquake occurrence.

[19] 2) Standard deviation of stress on the fault

$$SD(t) = \sqrt{\frac{1}{N}\sum_{i=1}^{N}[\tau_i(t) - AS(t)]^2}. \tag{1b}$$

The standard deviation gives an estimate for the range of fluctuations of stress on the fault. Increasing values correspond to increasing stress disorder and possible increasing proximity to a critical state.

[20] 3) Configurational entropy of stress on the fault

$$CE(t) = -\int p[s(t)]\ln\{p[s(t)]\}ds, \tag{1c}$$

where $p[s(t)]$ is the density distribution of stress on the fault at time t minus initial stress. The variable $CE(t)$, used previously by *Dahmen et al.* [1998], characterizes the evolving number of states of stress that are occupied on the fault at a given time. Increasing values correspond to stress distribution over broader range of states and possible increasing proximity to a critical state.

[21] 4) Order parameter based on stress fluctuations on the fault

$$SF(t) = \sqrt{\frac{1}{N}\sum_{i=1}^{N}(\tau_i(t) - \bar{\tau}_i)^2}, \tag{1d}$$

where $\bar{\tau}_i$ is the temporal average of stress at cell i during the entire deformation history. The variable $SF(t)$, motivated by a similar variable of *Ferguson* [1997] based on slip-deficit fluctuations in a block spring model, measures the temporal evolution of the RMS stress fluctuations on the fault. Increasing values correspond to increasing spatial correlation of stress fluctuations and possible increasing proximity to a critical state.

[22] 5) Two-dimensional power spectra of stress on the fault at different times minus initial stress. A distribution of power spectra over a broader range of scales corresponds to a possible increasing proximity to a critical state.

[23] There are clear conceptual overlaps between some of the stress functions. For example, the standard deviation, configurational entropy, and order parameter are different measurements of stress fluctuations and are expected in general to be in phase. In section 4 we analyze the correlations between the stress functions (1a)–(1d) for event groups in models F and FC.

2.3. Seismicity Functions

[24] The five seismicity functions are based on seven functions used by *Eneva and Ben-Zion* [1997a], along with a pattern recognition procedure, to characterize evolving seismicity in the space, time and size domains. *Eneva and Ben-Zion* [1997b] analyzed the evolution of the seven functions in relation to large events in synthetic earthquake catalogs generated by various realizations (including case F) of the model of *Ben-Zion* [1996]. The first 4 functions in the set used here are taken directly from Eneva and Ben-Zion and are calculated for overlapping groups of 100 events each moving forward in time by 20 events (and compared quantitatively with the first 4 stress functions calculated for the same groups). These choices provide a balance between temporal and statistical resolutions as discussed by *Eneva and Ben-Zion* [1997a, 1997b].

[25] The five employed seismicity functions are:

[26] 1) Spatial correlation dimension $CD(t_j)$ of hypocenter locations for event group j in different time windows ending at t_j. The value of CD is given by the slope of a straight segment in a double-logarithmic plot of

$$C_j(R) = \frac{p_j(r < R)}{P} = \frac{2p_j(r < R)}{N(N-1)}, \tag{2a}$$

where p_j is the number of event pairs in group j with distance $r < R$ and P is the total number of distinct pairs for N events (here $N = 100$ per group). The calculations of $C_j(R)$ and $CD(t_j)$ are done over certain distance ranges where scaling is observed. Following *Eneva and Ben-Zion* [1997b], we estimate $CD(t_j)$ for all event groups using a scaling distance range of 5–10 km. Larger values of CD indicate less spatial clustering (or increasing spatial diffusion) of hypocenters, compatible in general with increasing proximity to a critical state.

[27] 2) Average depth of hypocenter locations on the fault for event groups in different time windows

$$AZ(t_j) = \frac{1}{N}\sum_{t_{ji}}^{t_j} z(t), \tag{2b}$$

where z is the event depth and t_{ji} is the initial time of events in group j. Since the imposed boundary conditions (Figure 1a) tend to produce stress concentration and clustering of hypocenters at the bottom of the computational grid, local minima of $AZ(t_j)$ indicate increasing spatial diffusion of hypocenters and possible increasing proximity to a critical state.

[28] 3) Time interval for the occurrence of a given number (here 100) of earthquakes

$$TI(t_j) = t_j - t_{ji}. \tag{2c}$$

The temporal function TI is reciprocal to the seismicity rate. Increasing values of $TI(t_j)$ correspond to decreasing seismicity rates for which the term "seismic quiescence" is often used.

[29] 4) Ratio of number of events in different magnitude ranges for event groups in different time windows

$$MR(t_j) = \frac{n_j(M \geq M')}{n_j(M < M')}, \tag{2d}$$

where M', separating relatively small from relatively large events, is chosen to be 4.0 on the basis of properties of the frequency size statistics of earthquakes simulated by *Ben-Zion* [1996, Figure 15]. When the frequency size event statistics follow the Gutenberg-Richter power law distribution, $\log_{10}N(M \geq M') = a - bM'$, the function MR is the inverse of the b value. In general, however, determinations of b values are problematic and depend on the used magnitude range, tolerance level for deviations from pure power law distribution, estimation method, etc. In contrast, the function MR can be determined easily and unambiguously for any distribution. This is especially important for applications of the type done here with a small number ($N = 100$) of events, many of which not belonging to a power law range of frequency size statistics. Increasing values of $MR(t_j)$ correspond to broadening frequency size distribution and possible increasing proximity to a critical state.

[30] (5) For comparisons with more familiar parameters, we also examine temporal changes in a values, b values, and magnitude ranges of frequency size event statistics for larger groups, formed by stacking all earthquakes that occur within certain intervals prior to the large events. Increasing a values, decreasing b values, and increasing range of event statistics correspond to possible increasing proximity to a critical state.

[31] As with the stress functions, there are overlaps between some of the seismicity parameters. For examples, the spatial correlation dimension and average depth of hypocenters are expected to cluster or diffuse in phase, and the ratio of event numbers in different magnitude ranges is a generalization of the range of power law frequency size statistics. In section 4 we discuss the correlations between the seismicity functions (2a)–(2d) for models F and FC.

3. Stress Analysis at Individual Times

[32] Figure 2 illustrates the evolution of stress in the seismogenic zone of model F during a large earthquake cycle. Each frame shows the difference between stress at a given time and initial stress on the fault region 7.5 km $< x <$ 62.5 km, 4 km $< z <$ 8 km. Animation stressF of the stress evolution during the large earthquake cycle with higher density of frames is available as auxiliary material.[1] The stress is highly heterogeneous at all times, as is expected for all model realizations of the employed cellular (discrete) fault model. As discussed by *Ben-Zion* [1996], however, the short-scale stress roughening generated by the ongoing seismicity during a large earthquake cycle smoothes collectively the large-scale stress field. This prepares the fault (i.e., creates stress bridges that allow) for the occurrence of

[1] Supporting Animations are available at ftp://ftp.agu.org/append/jb/2002jb002121.

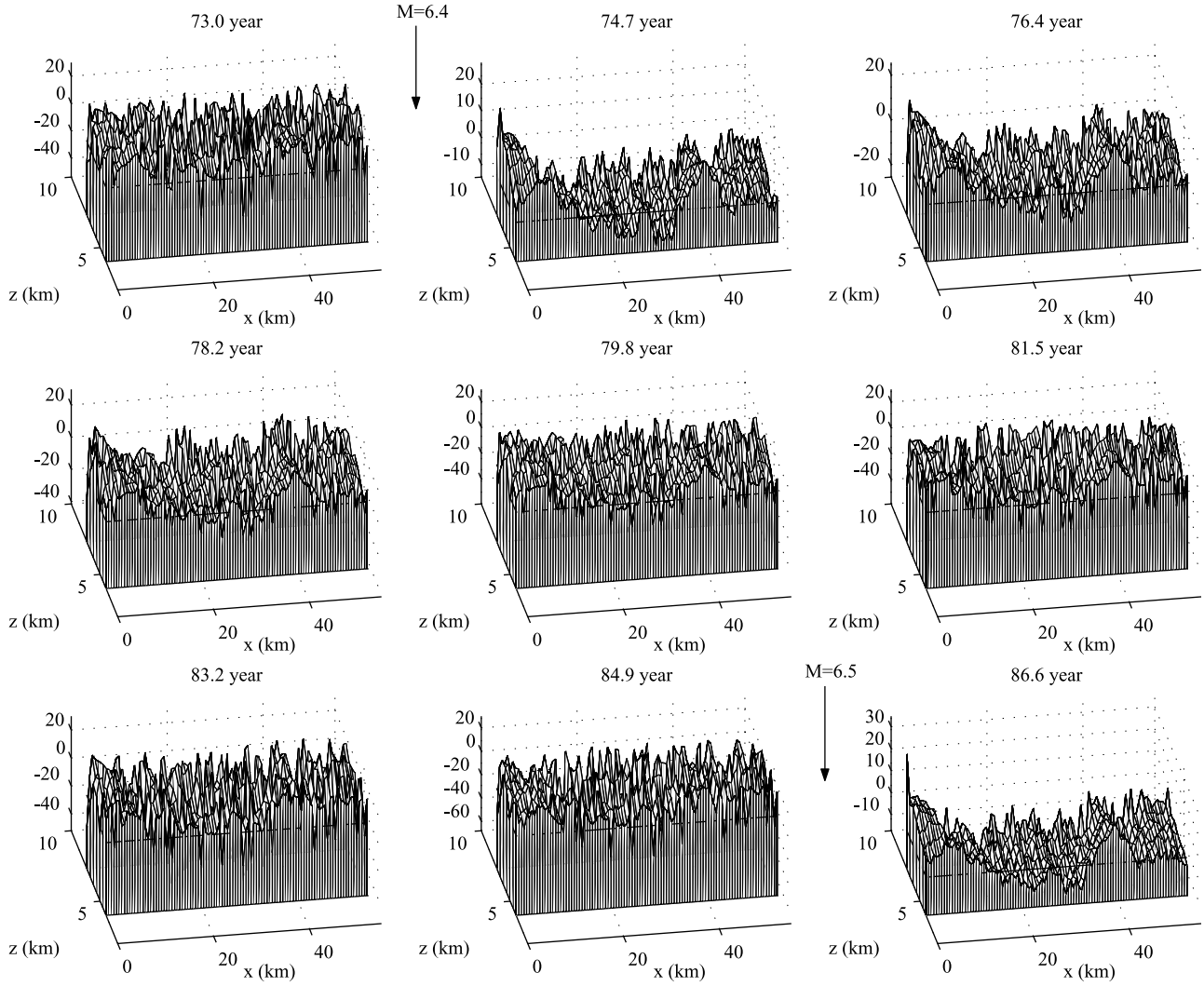

Figure 2. Stress minus initial stress on the central portion of the computational grid at different times in a large earthquake cycle for model F. The stress units are in bar with the zero level indicated by the flat surface. During the evolution leading to large events (arrows with magnitude values) the stress becomes rougher over relatively short length scales and smoother over relatively long ones. This trend is reversed during the occurrence of large events. Note changes of stress scale at different times. See also animation stressF with higher density, available as auxiliary material.

a large system-sized event. The above pattern of smoothing/roughening of long/short length scales of stress on the fault is reversed during the large system-sized failures.

[33] Figure 3 shows temporal evolution of functions (1a)–(1d) and seismicity in models F, FC, and SYS for about 10 years. Models F and SYS have one large earthquake cycle during that time interval and the cycle is clearly reflected in the structures of all functions. In contrast, the functions calculated for model FC exhibit a fractal-like behavior without preferred temporal scale or clear correspondence to the largest earthquakes in the examined time interval. The dramatic change from the cyclical structure of functions in model F to fractal-like signals in model FC illustrates the fundamental effect that the values of tuning parameters (here dynamic weakening) can have on the results. We also note that the ranges of values of the functions for model FC are considerably smaller than the ranges of values for models F and SYS.

[34] The large events in model F are separated by a magnitude gap from the other events and, as discussed by *Ben-Zion* [1996] and shown in the next section, the frequency size event statistics for this case are compatible with the characteristic earthquake distribution. (See *Ben-Zion and Rice* [1993] for explanation on the magnitude gap in terms of increasing stress concentration in elastic solid with the size of the failure area.) The seismicity plot for model FC has, in contrast, a smooth spread of events without magnitude gaps and, as discussed by *Fisher et al.* [1997] and illustrated in the next section, the frequency size event statistics for this case follow a (truncated) power law distribution. In model F with ongoing seismicity the functions fluctuate, especially toward the end of the large earthquake cycle, and have in general different phases than those of model SYS with only large events. In addition, the functions (1a)–(1d) reach in model F saturation levels within the large earthquake cycle that may be used, together

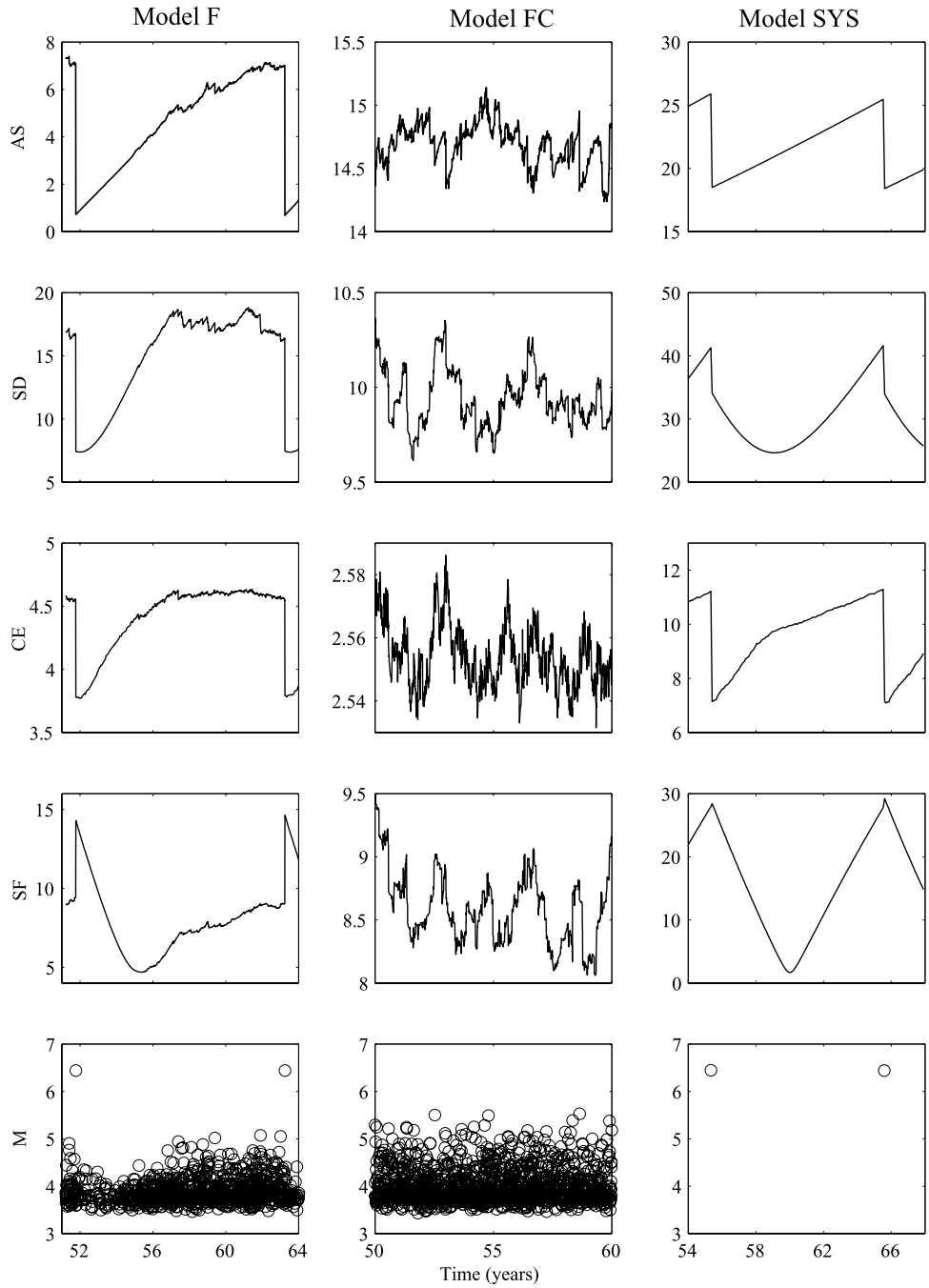

Figure 3. Evolution of stress functions (1a)–(1d) and seismicity in models F, FC, and SYS over about 10 years. The signals for AS, SD, and SF are in bar, and CE is nondimensional. The results for models F and SYS have clear cyclical components, while model FC produces fractal-like fluctuations.

with the increasing fluctuations of the time series, to mark the establishment of a condition for the occurrence of a future large event. In contrast, the evolution of these functions in model SYS, associated solely with the space-time-dependent loading, continues smoothly right up to the time of the future large event without precursory saturation and/or increasing fluctuations.

[35] Figures 4a–4d illustrate further the forgoing effects using longer time series of 150 years. In models F and SYS with dynamic weakening not at the critical value, the stress functions have clear cyclical structure associated with the times of the large events. In model FC with zero dynamic weakening, the functions are characterized by scale-invariant statistical fluctuations, without visible correlation to the large events, and smaller ranges of values than those generated by models F and SYS. The spikes of the stress fluctuation function *SF* at the large event times in models F and SYS are "after" (rather than precursory) effects produced by stress distributions associated with the large earthquakes. These spikes are suppressed by the analysis of event groups done in the next section.

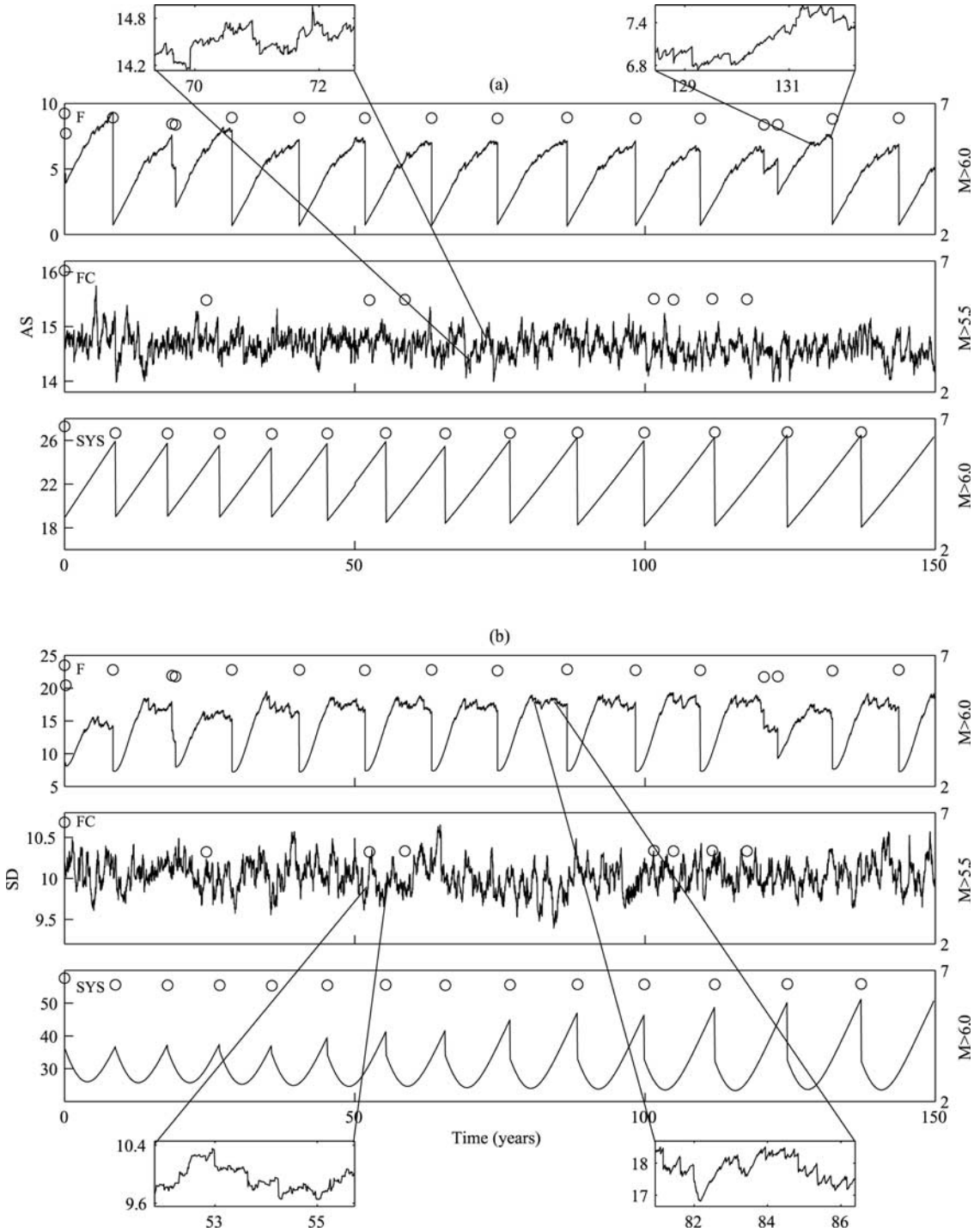

Figure 4. Evolution of stress functions (1a)–(1d) and large earthquakes (circles) in models F, FC, and SYS over 150 years. The results for models F and SYS show clear cyclical components, while the results for model FC show scale-invariant statistical fluctuations. The functions in model F become asymptotically stable and fluctuate before the occurrence of large events in contrast to the behavior in model SYS. The insets illustrate the similarity of functions in model F toward the end of cycles to those of model FC. The insets have (a) and (c) each 350 data points, (b) each 500 points, and (d) each 250 points.

[36] Early in the cycles, the evolution of the stress functions in model F is highly regular and similar to the evolution in model SYS. As time in a large earthquake cycle progresses, however, the stress functions in model F with ongoing seismicity develop increasing fluctuations in contrast to the smooth results of model SYS. In particular, following the establishment of saturation levels in functions (1a)–(1d), the fluctuations in model F increase and become

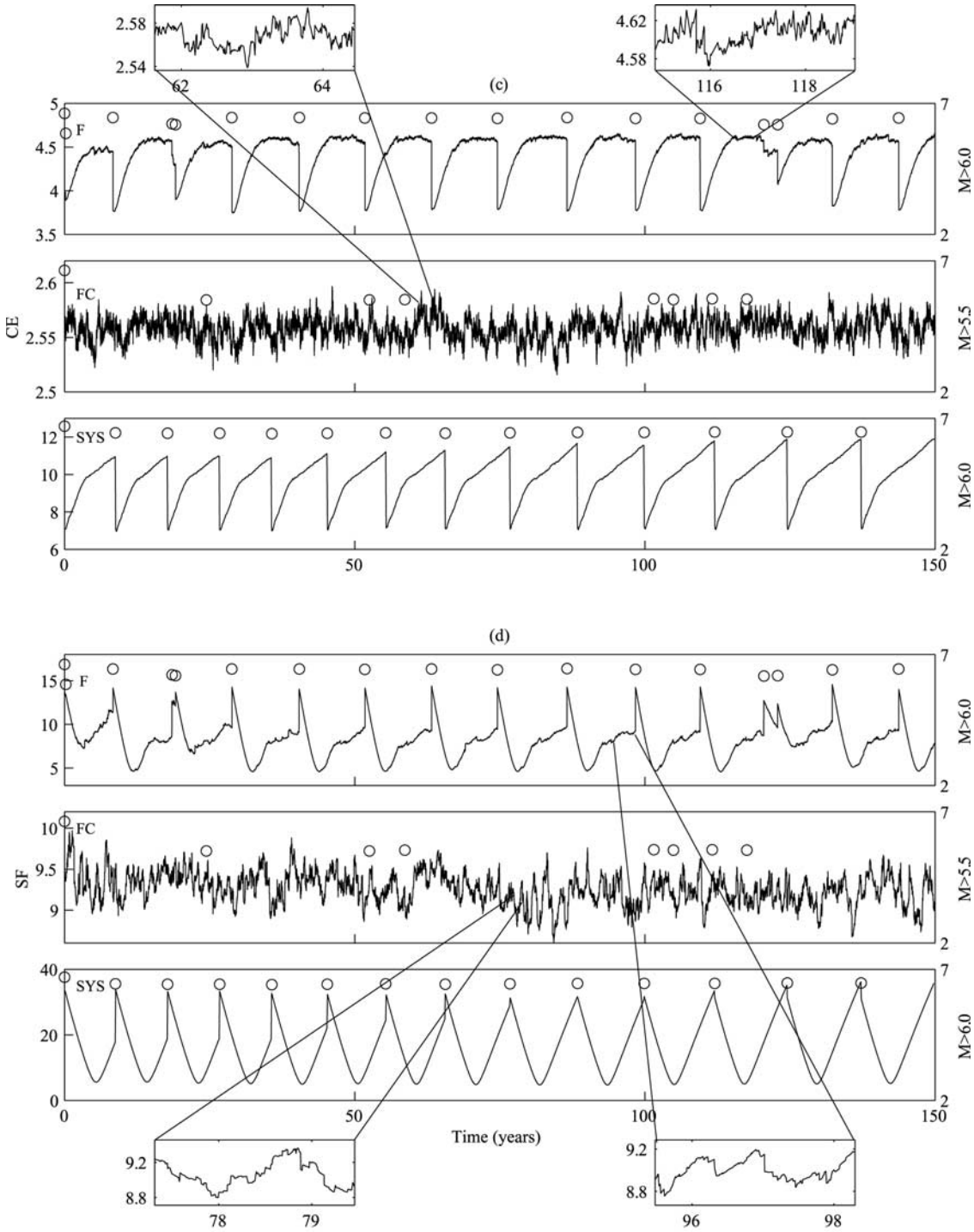

Figure 4. (continued)

similar to the scale-invariant signals of model FC. This is demonstrated in the insets of Figures 4a–4d, where it is seen that late in the cycle both the shapes and scales of fluctuations in model F are similar to those generated by model FC. The results suggest that the establishment of saturation in the stress functions for model F is associated with development of long-range correlations, and dynamic evolution of a tuning parameter related to strength − stress (or stress deficit) heterogeneity toward a critical value.

[37] Figure 5a shows evolving 2-D power spectra of stress in model F for the same large earthquake cycle of Figure 2. The zero wave number components have been removed from the results. Animation spectraF of the 2-D power spectra evolution with higher density of frames is available as auxiliary material. Early in the cycle, after the occurrence of a large event, the spectral energy is concentrated in long wavelength components on the order of the entire computational grid. The concentration of power

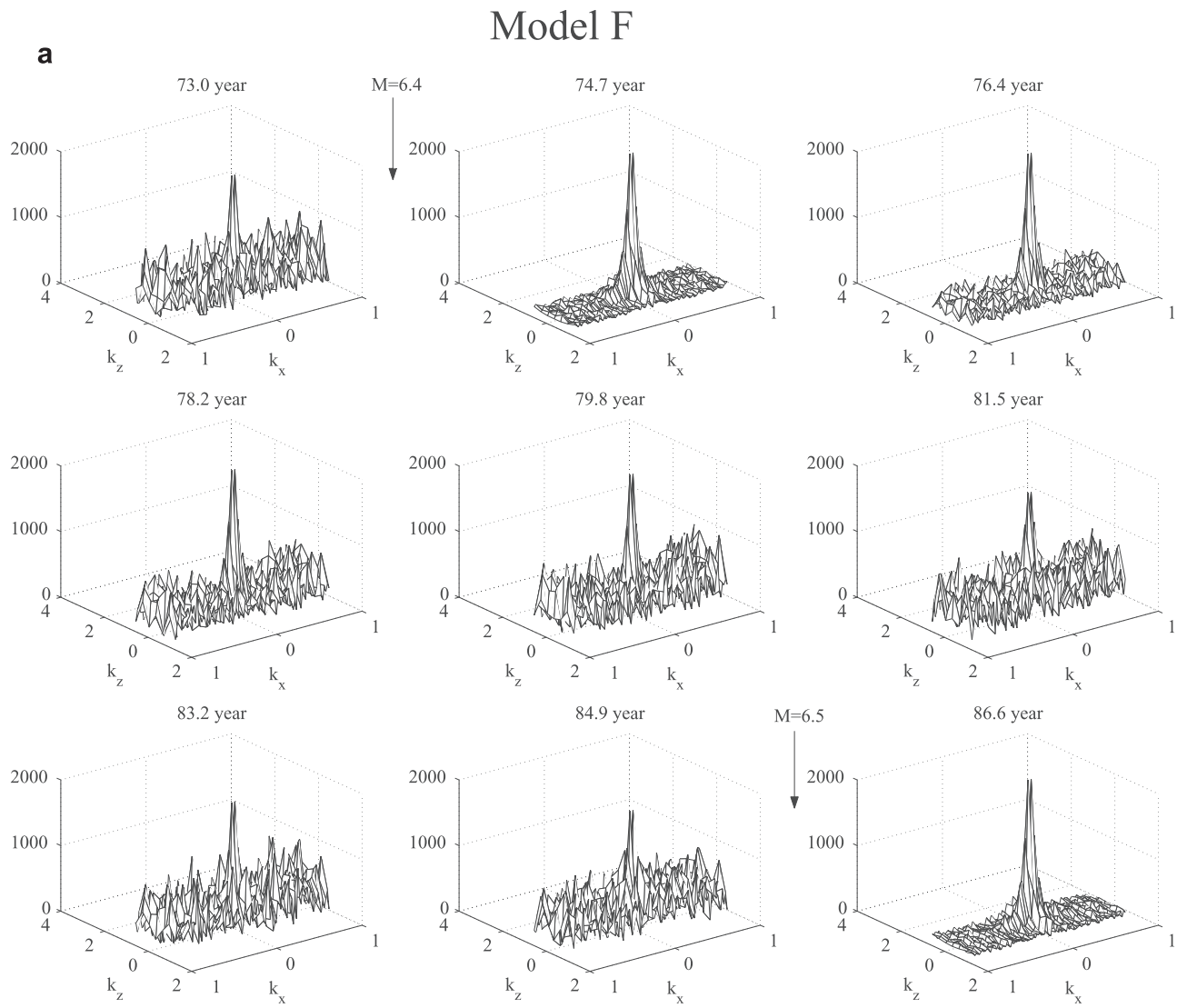

Figure 5. (a) Two-dimensional power spectra of stress for model F over horizontal (k_x) and vertical (k_z) wave numbers with the DC components removed. After the occurrence of large earthquakes, there are high central peaks produced by stress drops over long wavelengths. With time into the large earthquake cycle the power spectra become increasingly distributed over broad range of scales. (b) Same as Figure 5a but for model FC (note change of scale). Here the power spectra are broadly distributed at all times. (c) Same as Figure 5a but for model SYS (note change of scale). In this case the high central spectral peaks exist at all times. See also animations with higher density of frames, spectraF, spectraFC, and spectraSYS.

spectra in those long length scales is controlled by the boundary conditions and represents energy associated with the tectonic loading. The large spectral peak following a system-sized event is produced by a stress drop, or a negative stress change, over the scale of the system. The ongoing low and intermediate size events transfer stress spectral energy to smaller length scales and generate an increasingly broader range of scales as the cycle progresses in time. The cascade of stress spectral energy from large to small scales during a large earthquake cycle is analogous to the phenomenology of turbulence in fluid [e.g., *Frisch*, 1995]. However, the accompanying occurrence of increasingly larger events, discussed in the next section, produces an opposite cascade from small to large scales.

[38] Figures 5b and 5c show evolving 2-D power spectra of stress in models FC and SYS for about 10 years. Animations spectraFC and spectraSYS with higher density of frames are available as auxiliary material. In model SYS without evolving seismicity, the spectral energy remains concentrated at the long wavelength components at all times. The power spectra in the small length scales decreases toward the middle of the cycle and then increases back. This evolution is produced by the space-dependent loading (Figure 1a) and is also reflected in the behavior of functions *CD* and *SF* for model SYS in Figures 3 and 4. A similar evolutionary trend is present in model F as well, but is overcome there by the opposite evolution associated with the ongoing seismicity. In model FC with dynamic weakening at the zero critical value, the spectral energy is

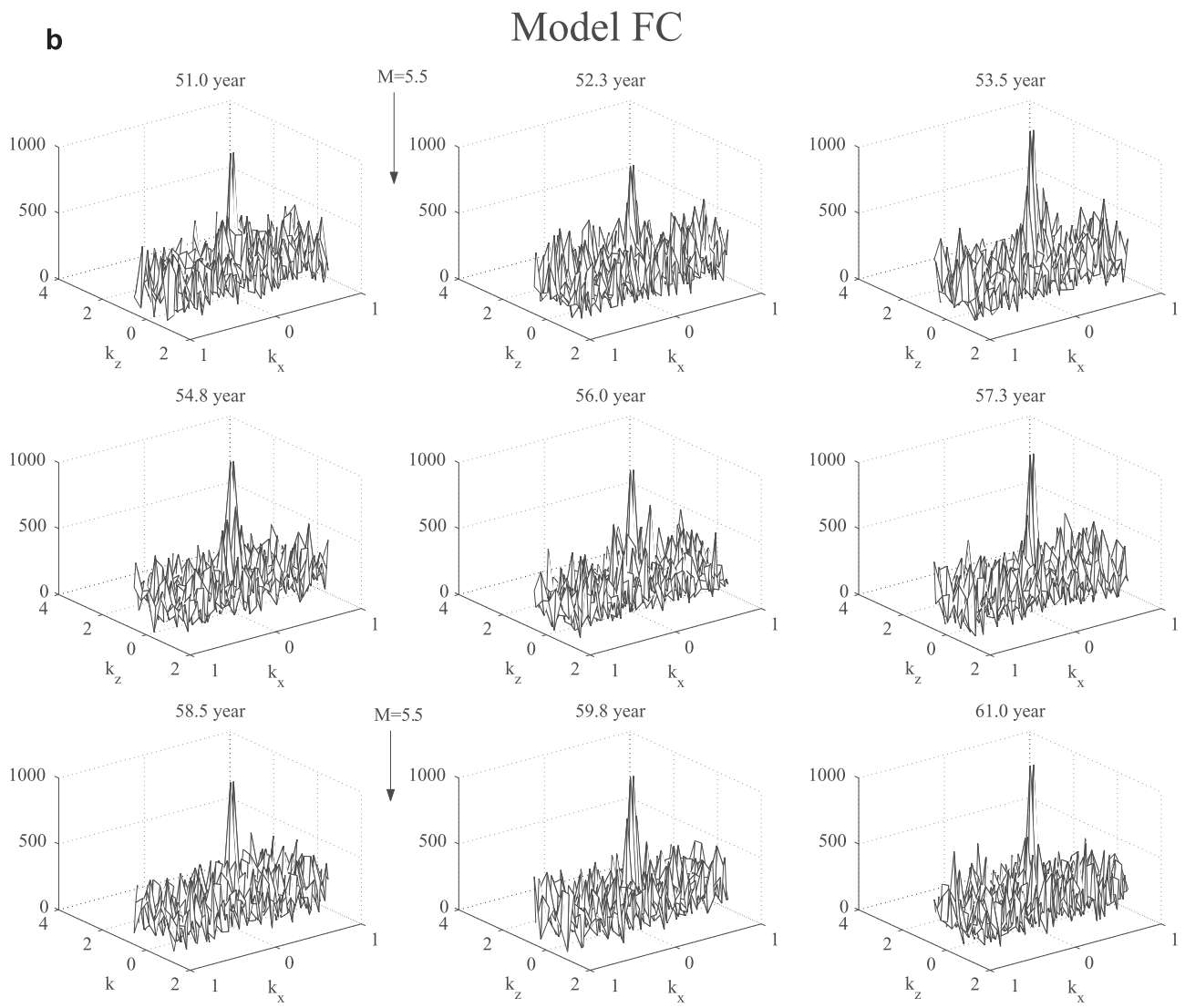

Figure 5. (continued)

distributed over a broad range of scales at all times. As discussed in the context of Figure 4, the evolution of power spectra in model F toward the end of a large earthquake cycle resembles in shape and scale the evolving spectral energy in model FC. These features are shown better in the animations (note the different scales in the different movies).

[39] The progression in model F from concentration of spectral energy over a narrow range of scales to a broad distribution with time into a large earthquake cycle is compatible with dynamic evolution toward an increasing proximity to a critical state. This is similar to what is assumed to occur in models of self-organized criticality [e.g., *Bak et al.*, 1988; *Bak and Tang*, 1989]. However, as discussed in the introduction and illustrated by the calculations for case FC, our model has tuning parameters in contrast to the premise of self-organized criticality [e.g., *Jensen*, 1998]. As mentioned above, the results for case F may be understood as associated with dynamic evolution of heterogeneity or disorder tuning parameter toward a critical value. This may explain why the results for model F toward the end of a large earthquake cycle are similar to the results for model FC with a critical value of the dynamic weakening tuning parameter. The behavior of model F appears to evolve during a large earthquake cycle from the response of the unrealistic model SYS with a small number of dynamic degrees of freedom, to the response of the unrealistic model FC with permanent criticality (and infinite number of dynamic degrees of freedom).

[40] The evolving spectral energy and stress functions for model F become asymptotically stable or saturate around 2/3–3/4 of a large earthquake cycle and then fluctuate until one event becomes the next system-sized earthquake and starts a new cycle. The configurational entropy generally saturates first and the average stress saturates last. The saturation of the evolving stress quantities corresponds physically to establishment of connectivity paths that enable a properly located hypocenter to propagate over the entire system. However, since the stress field is highly heterogeneous with many local minima of various sizes and shapes, the actual cascade of a brittle instability to a system-sized earthquake is a statistical event. Thus the

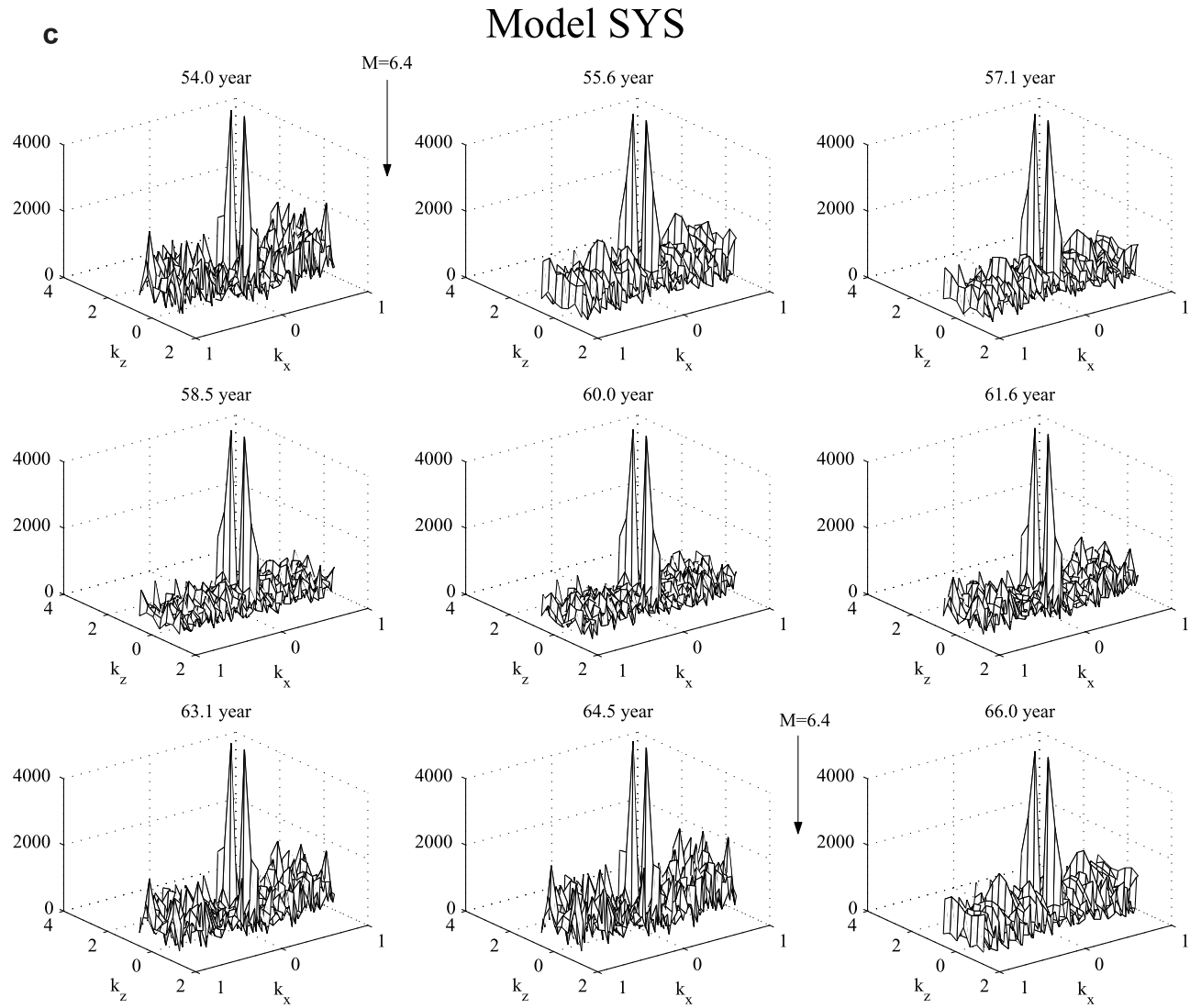

Figure 5. (continued)

smoothing of the long wavelength stress fluctuations and associated development of extrema in the examined functions provide a necessary but not a sufficient condition for the occurrence of a system-sized event.

[41] Since stress is not directly observable, it is important to find correlations between the features discussed above and corresponding analysis of seismicity signals. Also, as mentioned in section 2.2, the various stress functions are not independent of each other. In the next section we discuss correlations between the stress functions (1a)–(1d) calculated for groups of events, correlations between the seismicity functions (2a)–(2d) calculated for the same groups, and correlations between the stress and seismicity functions.

4. Seismicity and Stress Analysis for Groups of Events

[42] To analyze the temporal evolution of seismicity functions, we follow *Eneva and Ben-Zion* [1997b] and use overlapping groups of 100 events with a moving number window of 20 events. Thus every five consecutive groups share some events while the sixth group contains entirely new events. The seismicity functions can not be calculated for model SYS since it does not have event population between the large earthquakes. To compare the evolution of stress and seismicity functions in models F and FC, we analyze the stress functions for those models using identical event groups. To focus on the evolution preceding rather than following large events, we ignore the five consecutive groups after each large earthquake since those group values can be strongly affected by the stress distributions and changes of seismicity generated by the large events. As discussed by *Ben-Zion* [1996], earthquakes in model F with magnitude $M \geq 5.5$ are large events since they reduce the overall stress level in the computational grid rather than just redistributing it internally. Because of the lack of a cyclic structure in model FC, the size of large events in that model is determined on the basis of statistical rather than physical considerations. To have a similar ratio between the numbers of large events in models FC and F as the ratio (1.75) of the total numbers of events generated by the two models, we choose large events in model FC to be earthquakes with $M \geq 5.4$. With these choices, the number of examined groups for model F is 392 and for model FC it is 669.

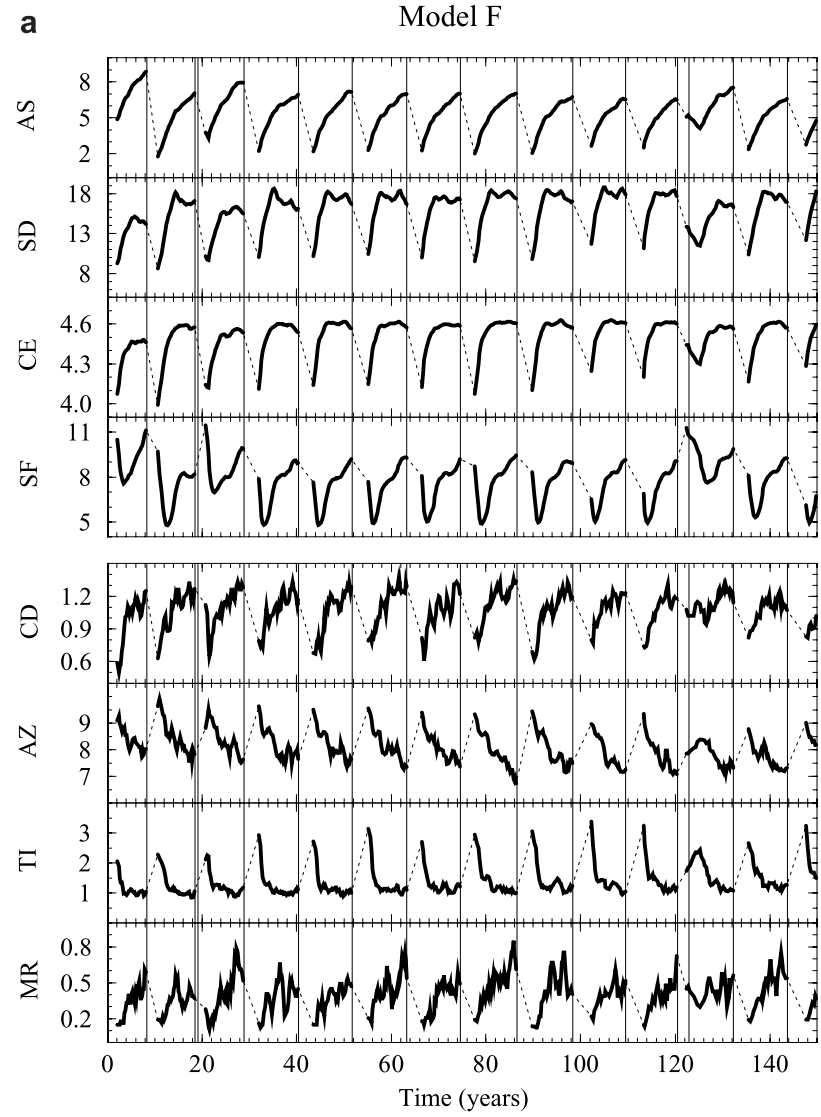

Figure 6. (a) Evolving group values of stress functions (1a)–(1d) and seismicity functions (2a)–(2d) for model F. Dashed segments interpolate over five ignored groups after each large ($M \geq 5.5$) earthquake (see text). Vertical lines indicate times of large events. The stress signals other than the nondimensional CE are in bar, CD and MR are nondimensional, AZ is in km, and TI is in year. The functions have cyclical behavior with increasing fluctuations and saturation or decreasing rate toward the end of each cycle. (b) Same as Figure 6a but for model FC with large events having $M \geq 5.4$. The results show scale-invariant statistical fluctuations.

[43] Figure 6a shows temporal evolution over 150 years of group stress and seismicity functions for model F together with the times of large events (thin vertical lines). Figure 6b gives similar results for 75 evolution years in model FC. The different timescales in Figures 6a and 6b are chosen to allow easier visual comparison between the results of the two models having significantly different overall number of events. As discussed in section 3 for evolving stress functions at individual times, the results for model F have a clear cyclical structure punctuated by the time of the large events, while the results for model FC appear to be characterized by scale-invariant statistical fluctuations. The group values of the standard deviation (*SD*) and configurational entropy (*CE*) of stress in model F reach saturation levels at about 1/2 to 2/3 of the large earthquake cycles and then fluctuate around those levels until the occurrence of a large event. The group values of the average stress (*AS*) and stress fluctuation (*SF*) continue to increase up or almost to the times of the large events.

[44] Since the seismicity functions in model F also follow a cyclical evolution associated with the large events, they track, with somewhat larger fluctuations, the evolution of the stress functions. The increasing values of the spatial correlation dimension (*CD*) during a large earthquake cycle indicate the occurrence of events over increasingly larger portions of the fault. This and the decreasing values of the average depth (*AZ*) point to hypocenter migration in a large earthquake cycle from the edges of the computational grid, where there are large stress concentrations at the start of the cycle, toward the center. The decreasing values of the time

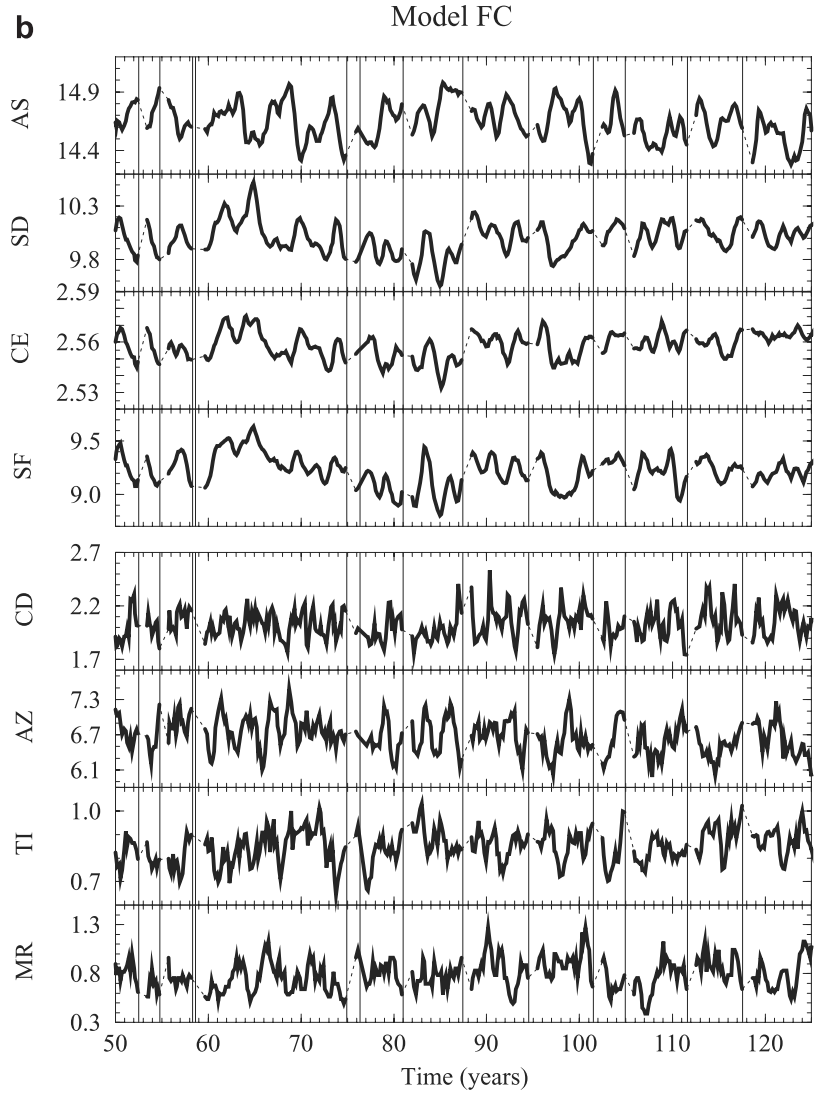

Figure 6. (continued)

interval (*TI*) of 100 events and increasing values of the magnitude ratio (*MR*) during a cycle are associated with increasing seismicity rates and event sizes with increasing proximity to large earthquake times. The overall level of *TI* in model F saturates at about 1/2 to 2/3 of the large earthquake cycles (Figure 6a). The values of *CD*, *AZ* and *MR* generally continue to evolve almost or up to the large event times, although *CD* and *MR* sometime saturate around 2/3 of the cycle. The seismicity functions for model FC show (Figure 6b) fractal-like fluctuations without clear correspondence to either the stress functions or the times of the large events. The seismicity functions in model F have increasing fluctuations and higher resemblance to the results of model FC toward the end of each cycle. The correlations between the stress and seismicity parameters in the two different models are examined more quantitatively below.

[45] To augment the estimates of the magnitude ratio *MR*, we calculate frequency size statistics of earthquakes stacked from four different time portions before the large model events. Figure 7a shows cumulative frequency size statistics of stacked events occurring in model F during the first, second, third, and forth quarters of the time intervals between large ($M \geq 5.5$) model earthquakes. (The large events themselves are not included in any portion.) Figure 7b gives corresponding results for frequency size event statistics from different portions of the time intervals between the large ($M \geq 5.4$) earthquakes in model FC. Figures 7c and 7d show the frequency size statistics of all events (including the large ones) in the 150-year catalogs for models F and FC, respectively. As seen in Figure 7c, the statistics for model F are compatible overall with the characteristic earthquake distribution. The results for model F show, however, clear evolution within large earthquake cycles (Figure 7a) manifested by increasing *a* values, decreasing *b* values, and increasing maximum and range of event sizes with approaching times of the large earthquakes. (Similar evolutionary trends can be discerned using rank order statistics [e.g., *Jaumé*, 2000].) In contrast, the statistics for model FC with dynamic weakening at the critical value follow both overall (Figure 7d) and at different time portions (Figure 7b) a power law distribution, modified by finite size effects associated with the minimum and maximum simulated events, without

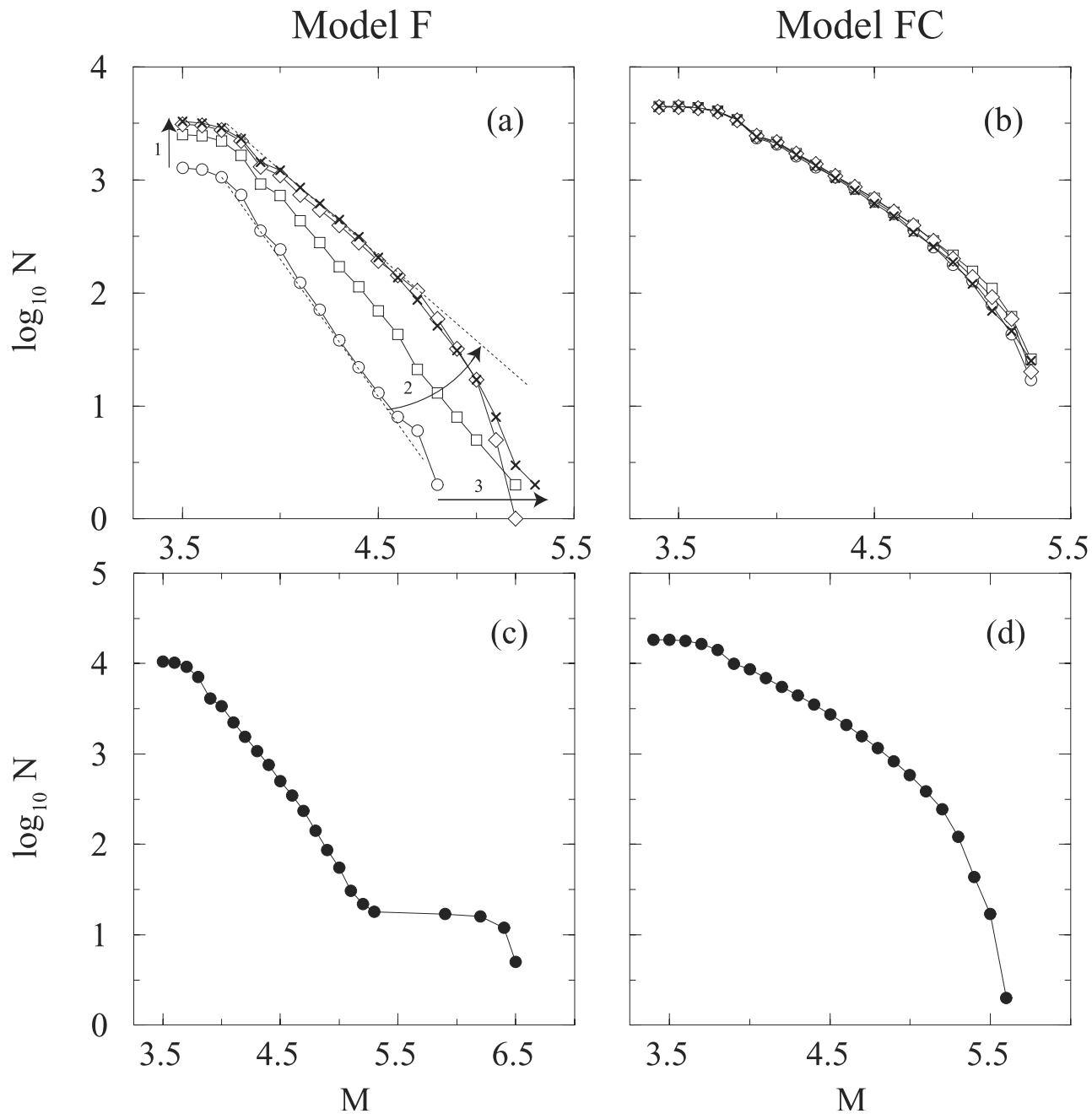

Figure 7. (a) Cumulative frequency-size statistics of events stacked from different portions of large earthquake cycles in model F. Results of stacked events from 0–25%, 25%–50%, 50%–75%, and 75%–100% of the time intervals between large earthquakes with $M \geq 5.5$ are denoted by circles, squares, diamonds, and crosses, respectively. The statistics show increasing a values (arrow 1), decreasing b values (arrow 2), and increasing maximum and range of events (arrow 3) as the large earthquake cycles progress. (b) Same as Figure 7a but for model FC with large events having $M \geq 5.4$. The results from all time intervals are similar and do not show evolution. (c) Cumulative frequency-size statistics of all events in 150-year history for model F. (d) Same as Figure 7c but for model FC.

evolutionary changes. The growing maximum event size during a large earthquake cycle in model F, and increasing ratio of relatively large to relatively small events reflected by the evolution of function *MR* in Figure 6a, form an opposite cascade to that occurring in turbulence as mentioned in section 3.

[46] Figures 8a and 8b show interparameter correlation plots for the stress functions (1a)–(1d) in models F and FC, respectively. Tables 1a and 1b list values of the interparameter correlations in models F and FC measured by linear and nonparametric rank order Spearman coefficients r_s. To examine evolutionary trends in the correlation plots, the last 10 group values before each large earthquake are plotted with a different symbol (+) than that of the other groups (o). The results indicate that the group values of most stress functions for model F (Figure 8a and Table 1a) are highly

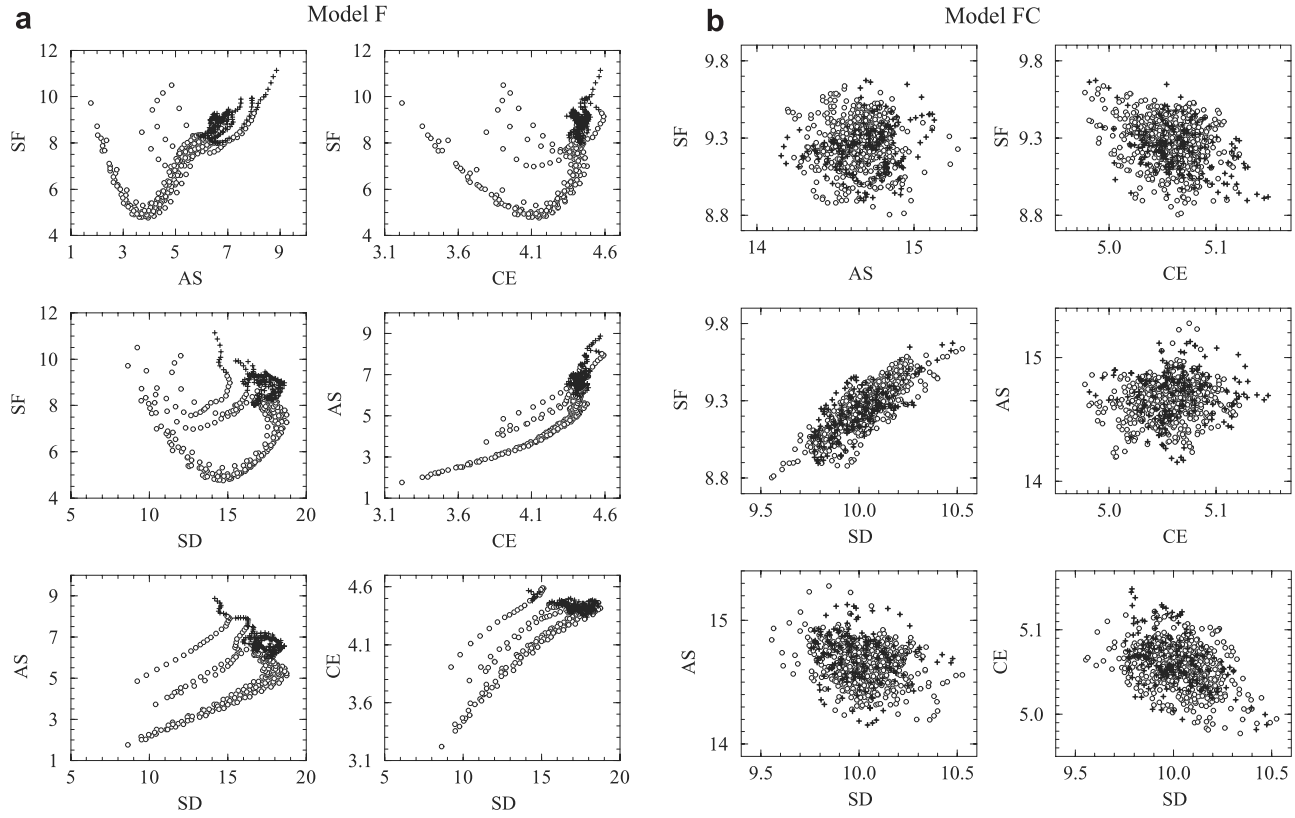

Figure 8. (a) Correlation plots of group stress functions (1a)–(1d) for model F. Plus signs mark values for the final 10 groups before each large event, and circles show the other group values. All parameters other than the nondimensional CE are in bar. Note the clear interparameter correlations and clustering before large earthquakes. The correlation coefficients are listed in Table 1a. (b) Same as Figure 8a but for model FC. Note the general lack of interparameter correlations and random appearance without relation to times of large events. The correlation coefficients are in Table 1b.

correlated (with $r_s > 0.8$ for the pairs *SF-AS* and *CE-SD*) and that the functions have clear evolution evidenced by the clustering of the final values before the large events. The existence of several nonoverlapping branches in Figure 8a reflects the fact that the large earthquake cycles in model F do not exactly repeat. The values in Figure 8a of the last 10 groups in each cycle occupy different portions of the branches and are significantly higher than the remaining group values, indicating a gradual progression of all stress functions during the cyclical evolution toward critical states. The apparent overlaps in the figure between the last 10 and other group values are produced by partial overlaps of the different branches. The corresponding results for model FC (Figure 8b and Table 1b) also show strong correlations between some of the stress functions ($r_s > 0.8$ for *SF-SD* and *CE-SD*). However, the final 10 values before the large events in Figure 8b do not occupy distinct portions of the correlation plots, indicating lack of persistent temporal evolution in model FC. We note that the last ten group values before large earthquakes in model F have a broader spread than other ten group values and produce more amorphous shapes similar to those generated by model FC.

[47] Figures 9a and 9b and Tables 2a and 2b give correlation plots and coefficients between the different seismicity functions. As discussed by *Eneva and Ben-Zion* [1997b], the seismicity functions in model F (Figure 9a and

Table 1a. Correlation Coefficients Between Stress Functions: Model F[a]

	SF	AS	CE
AS	0.82		
	(0.77)		
CE	0.37	0.40	
	(0.24)	(0.62)	
SD	0.16	0.22	0.89
	(0.18)	(0.51)	(0.97)

[a]Note: values with and without parentheses are, respectively, linear coefficients and nonparametric rank order Spearman correlation coefficients (r_s). The interparameter correlations can be significant even when the values of r_s are low [see *Eneva and Ben-Zion*, 1997b]. Coefficients smaller than 0.1 are marked with "–".

Table 1b. Correlation Coefficients Between Stress Functions: Model FC[a]

	SF	AS	CE
AS	–		
	(–)		
CE	0.57	−0.42	
	(0.59)	(−0.46)	
SD	0.81	−0.18	0.82
	(0.81)	(−0.22)	(0.83)

[a]Same as for Table 1a.

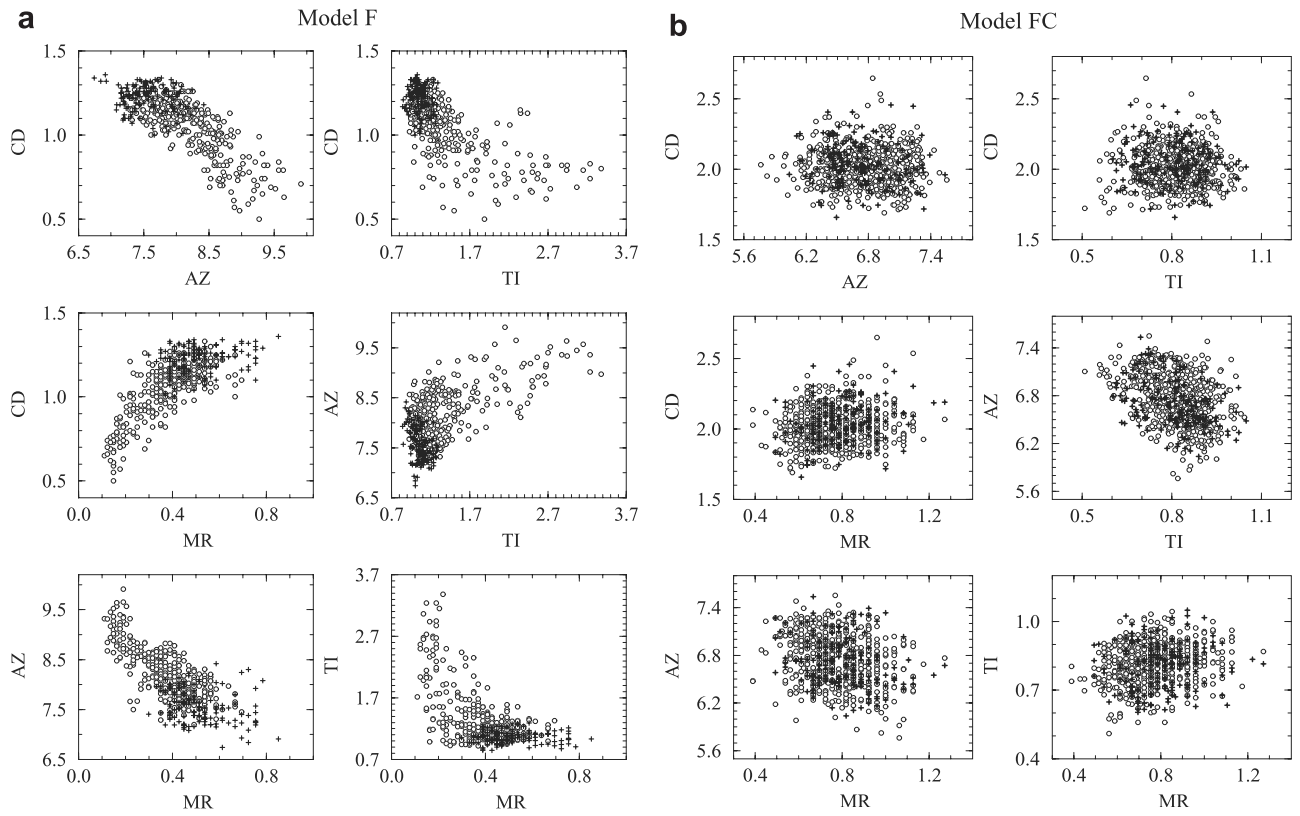

Figure 9. (a) Correlation plots of group seismicity functions (2a)–(2d) for model F. Symbols are as in Figure 8, CD and MR are nondimensional, AZ is in km, and TI is in year. The results show high correlations and clear cyclical evolution. The correlation coefficients are in Table 2a. (b) Same as Figure 9a but for model FC. The results show low correlations and lack of cyclical evolution. The correlation coefficients are in Table 2b.

Table 2a) have significant correlations (up to $r_s = -0.72$ for the *CD-AZ* pair), yet they are complementary rather than redundant. As with the stress functions, the last 10 values before each large event (+) cluster in distinct regions of the correlation plots, indicating clear overall cyclical evolution. In contrast, the results for model FC (Figure 9b and Table 2b) show considerably lower correlations and lack of persistent evolution. The shapes and spreads produced by the final ten groups in model F resemble those generated by model FC.

[48] An important goal of our work is to develop a rationale for using seismicity-based functions for tracking the evolution of stress on a fault. Figure 10a shows nine examples of correlation plots for pairs of stress and seismicity group values in model F. Table 3a gives the Spearman and linear correlation coefficients of all 16 stress-seismicity pairs formed by the stress functions (1a)–(1d) and seismicity functions (2a)–(2d). In agreement with the previous results and discussion, there are clear correlations between the stress and seismicity functions in model F, with $r_s > 0.7$ for the *CD-AS*, *AZ-CE* and *TI-AS* pairs. The data for the last 10 groups before large events cluster near the ends of the correlation plots, indicating coherent evolution toward critical values of both stress and seismicity functions during large earthquake cycles. In contrast, the correlation plots and coefficient values of the stress-seismicity pairs in model FC (Figure 10b and Table 3b) show weak or no correlations and lack of clear temporal evolution. In model FC, the seismicity functions provide little or no information on the evolving stress. While the overall shapes and ranges of values in the correlation plots of model F are different than those of model FC, the shapes and values produced by the last ten groups of model F resemble those of model FC.

Table 2a. Correlation Coefficients Between Seismicity Functions: Model F[a]

	CD	AZ	TI
AZ	−0.72		
	(−0.77)		
TI	−0.61	0.43	
	(−0.68)	(0.60)	
MR	0.69	−0.71	−0.46
	(0.74)	(−0.74)	(−0.57)

[a]Same as for Table 1a.

Table 2b. Correlation Coefficients Between Seismicity Functions: Model FC[a]

	CD	AZ	TI
AZ	–		
	(−)		
TI	–	−0.39	
	(−)	(−0.38)	
MR	0.14	−0.28	0.18
	(0.16)	(−0.28)	(0.17)

[a]Same as for Table 1a.

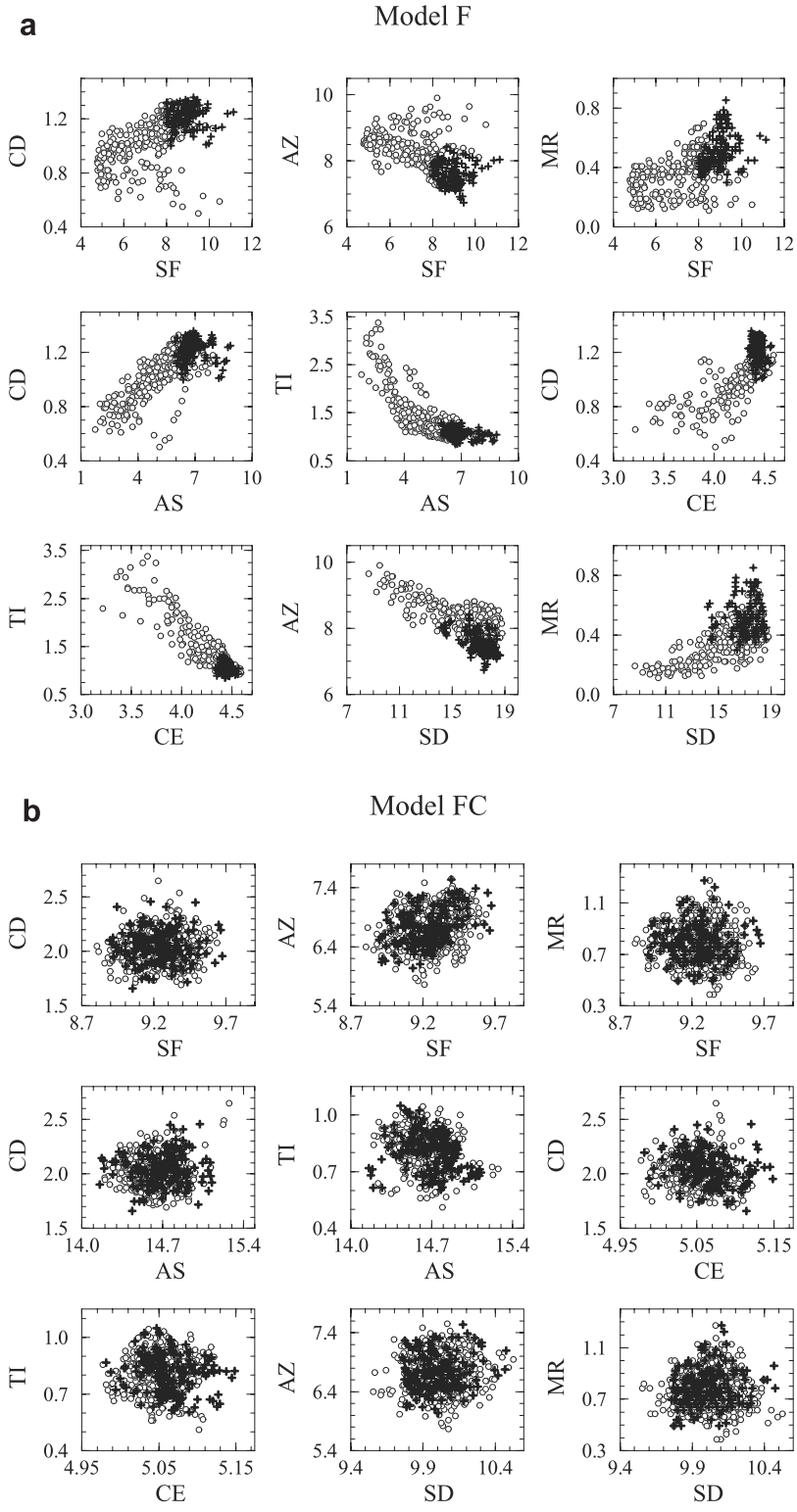

Figure 10. (a) Correlation plots for nine pairs of stress and seismicity group values for model F. Symbols and units are as in Figures 8 and 9. Note the high correlations between the stress and seismicity signals and clustering before large earthquakes. The correlation coefficients of all 16 pairs of stress and seismicity functions (1a)–(1d) and (2a)–(2d) are given in Table 3a. (b) Same as Figure 10a but for model FC. Note the low interparameter correlation and lack of persistent evolution. The correlation coefficients are in Table 3b.

Table 3a. Correlation Coefficients Between Seismicity and Stress Functions: Model F[a]

	SF	AS	CE	SD
CD	0.66	0.74	0.64	0.49
	(0.60)	(0.76)	(0.78)	(0.72)
AZ	−0.66	−0.66	−0.73	−0.58
	(−0.59)	(−0.71)	(−0.78)	(−0.72)
TI	−0.49	−0.73	−0.42	−0.31
	(−0.37)	(−0.78)	(−0.78)	(−0.71)
MR	0.57	0.63	0.63	0.54
	(0.55)	(0.67)	(0.68)	(0.64)

[a]Same as for Table 1a.

[49] Our seismicity functions are not necessarily the best possible surrogate variables for the stress functions. Nevertheless, if the calculated correlations for model F are indicative of those existing in nature, these observable functions may be used to follow the evolution of stress and development of large earthquake cycles on faults with realistic values of static and dynamic frictions.

5. Discussion

[50] The problem of earthquake prediction is of fundamental importance to both society and earthquake science. Progress in this problem is hampered, among other difficulties, by the facts that the governing dynamic variables like stress are not accessible for direct observations, and that instrumental observations of seismicity exist, even in the best cases, only for a fraction of a single large earthquake cycle. Overcoming these difficulties will require joint analyses of model and observed data. Examinations of long simulated histories of stress, slip, surface deformation, seismicity, and other variables of interest, for various types of models and ranges of model parameters, can provide a broader and deeper context for interpreting the limited and incomplete observed data.

[51] In the present work we analyze evolving stress and seismicity using the model of *Ben-Zion* [1996] for a large segmented strike-slip fault in a 3-D elastic half space. The model incorporates long-range elasticity, static/kinetic friction, power law creep, realistic boundary conditions, and quenched heterogeneities. The framework attempts to clarify the seismic response, on timescales of a few hundreds of years, of large individual fault systems occupying narrow and long spatial domains. As discussed by *Ben-Zion* [1996] and *Eneva and Ben-Zion* [1997b], the model results are compatible in general with many realistic features of brittle deformation along large faults, including stress profiles, hypocenter distributions, fault trace data, compiled earthquake statistics, and high-resolution microseismicity patterns.

[52] *Ben-Zion and Sammis* [2003] summarized multidisciplinary information on the geometrical and mechanical character of fault zones on the basis of field observations, laboratory data, and various model predictions. The results indicate that brittle failure of rock has an initial transient phase associated with strain hardening rheology, distributed deformation, and continual creation of new structures. However, with increasing deformation the response is replaced by strain weakening rheology and localization to tabular zones that become the main carriers of subsequent deformation. This structural evolution is accompanied by changes in the mechanical behavior of faults. Laboratory studies indicate that the static coefficient of friction for many crustal rocks is around 0.7 [*Byerlee*, 1978], in general agreement with stress measurements away from major faults [e.g., *McGarr and Gay*, 1978; *Brudy et al.*, 1997]. However, heat flow measurements along the San Andreas and other faults in California [e.g., *Brune et al.*, 1969; *Lachenbruch and Sass*, 1992] and additional evidence summarized by *Ben-Zion* [2001] indicate that large faults slip under considerably lower stress compatible with a dynamic coefficient of friction of 0.2 or less.

[53] The above studies imply that model realizations in the framework of *Ben-Zion* [1996] with a positive noncritical dynamic weakening, as case F, correspond to large mature faults like the San Andreas, North Anatolian, and Dead Sea transforms. On the other hand, model realizations with dynamic strengthening (not simulated here) correspond to deformation associated with immature faults in evolutionary stages preceding a throughgoing localization, or around barriers and other off-fault regions. The special case of model FC with a critical zero dynamic weakening (i.e., dynamic friction = static friction) corresponds to the transition between those two classes of deformation regimes and structures. Since large mature faults sustain the largest earthquakes (and are often near major urban areas), their dynamical behavior is of special relevance to seismic hazard.

[54] Our results indicate that on large mature faults with a positive dynamic weakening, the stress and seismicity coevolve during a large earthquake cycle toward a state resembling a critical phase transition. This is manifested by development of scale-invariant structures of dynamic fields, increasing correlation lengths of stress fluctuations and seismicity, and increasing ranges of stress power spectra and frequency size event statistics. These evolutionary trends are accompanied by increasing maximum earthquake size (and seismicity rate), in contrast to the large-to-small progression of event sizes in turbulence. However, during a large earthquake cycle the stress spectral energy is transferred from long to short length scales, and without a continual input of stress by the tectonic loading over the largest available scale the seismic activity will cease. Our model may thus be viewed as having both inverse (small-to-large) and direct (large-to-small) cascades. *Turcotte et al.* [1999] and *Gabrielov et al.* [1999] give detailed discussions of inverse and direct cascades of event sizes in the context of forest fire and other cellular automata models.

[55] The evolving stress and seismicity functions for model F become asymptotically stable or saturate around

Table 3b. Correlation Coefficients Between Seismicity and Stress Functions: Model FC[a]

	SF	AS	CE	SD
CD	–	–	–	–
	(–)	(–)	(–)	(–)
AZ	0.34	0.31	–	0.14
	(0.34)	(0.34)	(–)	(0.14)
TI	−0.28	−0.18	–	–
	(−0.30)	(−0.24)	(–)	(–)
MR	–	–	–	–
	(–)	(–)	(–)	(–)

[a]Same as for Table 1a.

1/2–3/4 of a large earthquake cycle, depending on the examined quantity, and then fluctuate until one hypocenter cascades to become the next system-size event. The actual saturation times are related to the employed (finite) size of the fault and assumed constitutive parameters. For a given fault size and rheological properties, the saturation of the evolving stress quantities corresponds to establishment of connecting paths (and long-range correlations) through the heterogeneous stress field. These connections smooth collectively the stress topography over large length scales and allow a properly located hypocenter to propagate over the entire system. Since the stress field is highly heterogeneous over short length scales, however, the nucleation of brittle instability in a position leading to a system-sized earthquake is a statistical event. Thus the smoothing of the large-scale stress components, the establishment of long-range correlations, and the proximity of stress deficit disorder to a critical level, provide a necessary but not a sufficient condition for a system-sized event. The occurrence of a large earthquake starts a new cycle manifested by concentration of stress spectral energy in long (system-sized) wavelengths, initial evolution of seismicity and stress functions along regular (quasi linear and parabolic) dynamic structures, short correlation lengths of stress and seismicity, and narrow range of frequency size statistics. Regional earthquakes produce additional perturbations to the evolving stress and seismicity, not accounted for in our calculations, but those do not change the essential character of the evolutionary process itself and large earthquake cycle on a fault.

[56] The discussed evolution may be characterized overall as intermittent criticality. This is different from self-organized criticality by the existence of cyclical evolution and tuning parameters, both of which can be highly important for possible forecasting of large events. The results are in general agreement with calculations of *Heimpel* [1997] based on a model similar to ours, cellular automata simulations of *Sammis and Smith* [1999], *Weatherley et al.* [2002], and *Main et al.* [2000], block spring calculations of *Kumagai et al.* [1999], and analyses of *Rundle et al.* [1999] and *Klein et al.* [2000] with several types of models. In self-organized criticality, the behavior is characterized solely by statistical fluctuations around a critical state [e.g., *Bak et al.*, 1988; *Main*, 1996; *Jensen*, 1998]. This type of evolution exists in the special model realization FC, where we set the dynamic weakening parameter to the critical zero value. However, in the more general and more realistic model F with a finite positive dynamic weakening, the evolution is richer and has, in addition to statistical fluctuations, an overall cyclical structure.

[57] It is important to distinguish between self-organized criticality and (intermittent) criticality, since proper recognition and understanding of tuning parameters may be used to organize observed data in categories associated with different dynamic regimes. This can reduce the apparent complexity of the data and enhance potentially informative signals. Our results suggest, in agreement with *Ben-Zion and Rice* [1993, 1995] and *Ben-Zion* [1996], that the range of size scales characterizing fault heterogeneities may act as a tuning parameter of the dynamics, with increasing range corresponding to increasing proximity to criticality. In model F and corresponding cases in nature (possibly the San Andreas and other relatively straight faults), with a narrow range of strength heterogeneities, the evolution toward a critical state during a large earthquake cycle is produced by stress fluctuations over increasing ranges of scales. In model realizations with a broad range of strength heterogeneities, like case M of *Ben-Zion* [1996], and corresponding cases in nature (possibly the San Jacinto and other disordered faults), the dynamics may be closer to or at a critical state at all times as in model FC. The data on geometrical properties of faults summarized by *Ben-Zion and Sammis* [2003] suggest that faults evolve during their active lifetime from the latter class to the former.

[58] The results of section 4 indicate that monitoring changes of the seismicity functions (2a)–(2d) may be used as a proxy for the evolution of stress and a large earthquake cycle on a heterogeneous fault. These functions are not necessarily the best surrogate variables for stress and large seismic cycles and they should be augmented by other functions that provide useful information on evolving deformation. Possible examples include the degrees of spatial nonrandomness of hypocenters and event repetitiveness of *Eneva and Ben-Zion* [1997a, 1997b], cumulative Benioff strain [e.g., *Bufe and Varnes*, 1993; *Bowman et al.*, 1998; *Jaumé and Sykes*, 1999], evolving correlations of hypocenter distributions [*Zöller and Hainzl*, 2002], and other signals used in the prediction algorithms of *Keilis-Borok and Kossobokov* [1990], *Kossobokov et al.* [2000], *Pepke et al.* [1994], and *Rundle et al.* [2000]. Continuing studies of evolving dynamic variables and observable response functions like seismicity and surface deformation in model simulations can improve the physical basis for understanding large earthquake cycles. Combined analysis of results from such studies and observed data may lead to the development of improved prediction algorithms, having shorter time windows of increased probability for the occurrence of large events and higher performance reliability.

[59] **Acknowledgments.** The studies were supported by a Zumberge research fund of USC and the National Earthquake Hazard Reduction Program of the USGS (Grant number 02HQGR0047). We thank Marian Anghel for useful comments on an early version of the paper. The manuscript benefited from additional comments by Steve Jaume', anonymous referee and associate editor, and Francis Albarède.

References

Bak, P., and C. Tang, Earthquakes as a self-organized critical phenomenon, *J. Geophys. Res.*, *94*, 15,635–15,637, 1989.

Bak, P., C. Tang, and K. Wiesenfeld, Self-organized criticality, *Phys. Rev. E*, *38*, 364–374, 1988.

Ben-Zion, Y., Stress, slip and earthquakes in models of complex single-fault systems incorporating brittle and creep deformations, *J. Geophys. Res.*, *101*, 5677–5706, 1996.

Ben-Zion, Y., Dynamic rupture in recent models of earthquake faults, *J. Mech. Phys. Solids*, *49*, 2209–2244, 2001.

Ben-Zion, Y., and J. R. Rice, Earthquake failure sequences along a cellular fault zone in a three-dimensional elastic solid containing asperity and nonasperity regions, *J. Geophys. Res.*, *98*, 14,109–14,131, 1993.

Ben-Zion, Y., and J. R. Rice, Slip patterns and earthquake populations along different classes of faults in elastic solids, *J. Geophys. Res.*, *100*, 12,959–12,983, 1995.

Ben-Zion, Y., and J. R. Rice, Dynamic simulations of slip on a smooth fault in an elastic solid, *J. Geophys. Res.*, *102*, 17,771–17,784, 1997.

Ben-Zion, Y., and C. G. Sammis, Characterization of fault zones, *Pure Appl. Geophys.*, *160*, 677–715, 2003.

Ben-Zion, Y., K. Dahmen, V. Lyakhovsky, D. Ertas, and A. Agnon, Self-driven mode switching of earthquake activity on a fault system, *Earth Planet. Sci. Lett.*, *172*, 11–21, 1999.

Bowman, D. D., G. Ouillon, C. G. Sammis, A. Sornette, and D. Sornette, An observational test of the critical earthquake concept, *J. Geophys. Res.*, *103*, 24,359–24,372, 1998.

Brudy, M., M. D. Zoback, K. Fuchs, F. Rummel, and J. Baumgaertner, Estimation of the complete stress tensor to 8 km depth in the KTB scientific drill holes: Implications for crustal strength, *J. Geophys. Res.*, *102*, 18,453–18,475, 1997.

Brune, J. N., T. L. Henyey, and R. F. Roy, Heat flow, stress and rate of slip along the San Andreas Fault, California, *J. Geophys. Res.*, *74*, 3821–3827, 1969.

Bufe, C. G., and D. J. Varnes, Predictive modeling of the seismic cycle of the great San Francisco bay region, *J. Geophys. Res.*, *98*, 9871–9883, 1993.

Byerlee, J. D., Friction of rocks, *Pure Appl. Geophys.*, *116*, 615–626, 1978.

Chinnery, M., The stress changes that accompany strike-slip faulting, *Bull. Seismol. Soc. Am.*, *53*, 921–932, 1963.

Dahmen, K., D. Ertas, and Y. Ben-Zion, Gutenberg Richter and characteristic earthquake behavior in simple mean-field models of heterogeneous faults, *Phys. Rev. E*, *58*, 1494–1501, 1998.

Dieterich, J. H., Earthquake nucleation on faults with rate- and state-dependent strength, *Tectonophysics*, *211*, 115–134, 1992.

Eneva, M., and Y. Ben-Zion, Techniques and parameters to analyze seismicity patterns associated with large earthquakes, *J. Geophys. Res.*, *102*, 17,785–17,795, 1997a.

Eneva, M., and Y. Ben-Zion, Application of pattern recognition techniques to earthquake catalogs generated by models of segmented fault systems in three-dimensional elastic solids, *J. Geophys. Res.*, *102*, 24,513–24,528, 1997b.

Ferguson, C. D., Numerical investigations of an earthquake fault based on a cellular automaton, slider-block model, Ph. D. diss., Boston Univ., Boston, Mass., 1997.

Fisher, D. S., K. Dahmen, S. Ramanathan, and Y. Ben-Zion, Statistics of earthquakes in simple models of heterogeneous faults, *Phys. Rev. Lett.*, *78*, 4885–4888, 1997.

Frisch, U., *Turbulence: The Legacy of A. N. Kolmogorov*, Cambridge Univ. Press, New York, 1995.

Gabrielov, A., W. I. Newman, and D. L. Turcotte, Exactly soluble hierarchical clustering model: Inverse cascades, self-similarity, and scaling, *Phys. Rev. E*, *60*, 5293–5300, 1999.

Heimpel, M., Critical behavior and the evolution of fault strength during earthquake cycles, *Nature*, *388*, 865–868, 1997.

Jaumé, S. C., Changes in earthquake size-frequency distributions underlying accelerating seismic moment/energy release, in *GeoComplexity and the Physics of Earthquakes*, *Geophys. Monogr. Ser.*, vol. 120, edited by J. B. Rundle, D. L. Turcotte, and W. Klein, pp. 199–210, AGU, Washington, D. C., 2000.

Jaumé, S. C., and L. R. Sykes, Evolving toward a critical point: A review of accelerating seismic moment/energy release prior to large and great earthquakes, *Pure Appl. Geophys.*, *155*, 279–305, 1999.

Jensen, H. J., *Self-Organized Criticality*, Cambridge Univ. Press, New York, 1998.

Keilis-Borok, V. I., and V. G. Kossobokov, Premonitory activation of earthquake flow: Algorithm M8, *Phys. Earth Planet. Inter.*, *61*, 73–83, 1990.

Klein, W., M. Anghel, C. D. Ferguson, J. B. Rundle, and J. S. Sá Martins, Statistical analysis of a model for Earthquake faults with long-range stress transfer, in *GeoComplexity and the Physics of Earthquakes*, *Geophys. Monogr. Ser.*, vol. 120, edited by J. B. Rundle, D. L. Turcotte, and W. Klein, pp. 43–71, AGU, Washington, D. C., 2000.

Kossobokov, V. G., V. I. Keilis-Borok, D. L. Turcotte, and B. D. Malamud, Implications of a statistical physics approach for earthquake hazard assessment and forecasting, *Pure Appl. Geophys.*, *157*, 2323–2349, 2000.

Kumagai, H., Y. Fukao, S.-I. Watanabe, and Y. Baba, A self-organized model of earthquakes with constant stress drops and the b-value of 1, *Geophys. Res. Lett.*, *26*, 2817–2820, 1999.

Lachenbruch, A. H., and J. H. Sass, Heat flow from Cajon Pass, fault strength and tectonic implications, *J. Geophys. Res.*, *97*, 4995–5030, 1992.

Lyakhovsky, V., Y. Ben-Zion, and A. Agnon, Earthquake cycle, fault zones, and seismicity patterns in a rheologically layered lithosphere, *J. Geophys. Res.*, *106*, 4103–4120, 2001.

Main, I., Statistical physics, seismogenesis, and seismic hazard, *Rev Geophys.*, *34*, 433–462, 1996.

Main, I. G., G. O'Brien, and J. Henderson, Statistical physics of earthquakes: Comparison of distribution exponents for source area and potential energy and the dynamic emergence of log-periodic energy quanta, *J. Geophys. Res.*, *105*, 6105–6126, 2000.

McGarr, A., and N. C. Gay, State of stress in the Earth's crust, *Annu. Rev. Earth Planet. Sci.*, *6*, 405–436, 1978.

Pepke, S. L., J. M. Carlson, and B. E. Shaw, Prediction of large events on a dynamical model of a fault, *J. Geophys. Res.*, *99*, 6769–6788, 1994.

Rice, J. R., Spatio-temporal complexity of slip on a fault, *J. Geophys. Res.*, *98*, 9885–9907, 1993.

Rundle, J. B., W. Klein, and S. Gross, Physical basis for statistical patterns in complex earthquake populations: Models, predictions and tests, *Pure Appl. Geophys.*, *155*, 575–607, 1999.

Rundle, J. B., W. Klein, K. Tiampo, and S. Gross, Linear pattern dynamics in nonlinear threshold system, *Phys. Rev. E*, *61*, 2418–2431, 2000.

Sammis, C. G., and S. W. Smith, Seismic cycles and the evolution of stress correlation in cellular automaton models of finite fault networks, *Pure Appl. Geophys.*, *155*, 307–334, 1999.

Scholz, C. H., *The Mechanics of Earthquakes and Faulting*, 2nd ed., Cambridge Univ. Press, New York, 2002.

Shaw, B. E., and J. R. Rice, Existence of continuum complexity in the elastodynamics of repeated fault ruptures, *J. Geophys. Res.*, *105*, 23,791–23,810, 2000.

Sornette, D., and C. G. Sammis, Complex critical exponents from renormalization group theory of earthquakes: Implications for earthquake predictions, *J. Phys. Paris*, *5*, 607–619, 1995.

Turcotte, D. L., B. E. Malamud, G. Morein, and W. I. Newman, An inverse-cascade model for self-organized critical behavior, *Physica A*, *268*, 629–643, 1999.

Weatherley, D., P. Mora, and M. F. Xia, Long-range automaton models of earthquakes: Power-law accelerations, correlation evolution, and mode-switching, *Pure Appl. Geophys.*, *159*, 2469–2490, 2002.

Zöller, G., and S. Hainzl, A systematic spatiotemporal test of the critical point hypothesis for large earthquakes, *Geophys. Res. Lett.*, *29*(11), 1558, 10.1029/2002GL014856, 2002.

Zöller, G., M. Holschneider, and Y. Ben-Zion, Quasi-static and quasi-dynamic modeling of earthquake failure at intermediate scales, *Pure Appl. Geophys*, in press, 2003.

Y. Ben-Zion and Y. Liu, Department of Earth Sciences, University of Southern California, Los Angeles, CA 90089-0740, USA. (yunfengl@terra.usc.edu; benzion@terra.usc.edu)

M. Eneva, Science Applications International Corporation, San Diego, CA 92121, USA. (Mariana.Eneva@saic.com)